

predictable relationship between the intensity of reflected light at a point and the image gray level. With radar imagery, there are corresponding effects. Geometric distortion can occur because of inaccuracies in the relationship between time delay and ground range in the crosstrack direction or, for SAR, between Doppler shift and ground range in the along-track dimension. Both of these distortions tend to be negligible when vehicle trajectory is well known (e.g., as with a satellite). Camera spot size corresponds to SAR resolution in both crosstrack and along-track dimensions; camera Airey-ring amplitude corresponds to SAR side-lobe levels. The relationship between brightness and

gray level in film corresponds to the dynamic range limitations in the radar receiver. The present and predicted performance parameters for RAR and SAR are summarized in table 5-III.

A typical SAR that would be suitable for the Space Shuttle and that has three frequencies, two polarizations, and other aforementioned parameters is described in a subsequent section. The satellite portion of such a radar will weigh approximately 500 kg and require 2 kW of prime power.

A general system description and tradeoff considerations for real aperture side-looking airborne radar (SLAR) are presented in part B.

N76 11825

PART B

EXAMPLES OF CURRENT RADAR TECHNOLOGY AND APPLICATIONS

USE OF SLAR FOR EARTH RESOURCES MAPPING

The design and manufacture of SLAR evolved primarily from requirements established by military users. In recent years, emphasis has been directed toward improved moving-target detection and higher resolution fixed-target capabilities. Improvements in both these parameters are important for tactical applications; however, the applicability of state-of-the-art military systems to the general remote-sensing problem is not well established.

The potential of SLAR for Earth and ocean remote-sensing applications has begun to emerge only in the past decade. Earth scientists and engineers have found that the radar map is an extremely useful tool. To the casual observer, a radar map may appear very similar to high-resolution photographs and may seem to warrant similar interpretations. However, full use of the data available in radar imagery requires a general understanding of the operating principles of SLAR and the microwave reflectivity char-

acteristics of the terrain being mapped. The radar imagery will enhance certain features and suppress others.

This section briefly summarizes the basic principles and tradeoff considerations for SLAR. There are two fundamental types of SLAR sensors available to the remote-sensing user: real aperture and synthetic aperture. The primary difference between the two types is that a synthetic aperture system is capable of significant improvements in target resolution but requires equally significant added complexity and cost. The remote-sensing users must have a good understanding of the resolution required for each sensing mission.

The advantages of real aperture SLAR include long-range coverage, all-weather operation, in-flight processing and image viewing, and lower cost. The fundamental limitation of the real aperture approach is target resolution. However, the RAR is well suited for airborne missions that require real-time data with moderate resolution.

Synthetic aperture processing is the most practical approach for remote-sensing prob-

lems that require higher resolution (more than 30 to 40 m). However, various synthetic aperture design approaches are available, depending on the degree of resolution required. To obtain resolution improvement, sacrifices must often be made regarding range coverage, in-flight processing, and cost.

During the next 5 to 10 yr, the use of SLAR for remote sensing should expand dramatically. Based on known requirements, it appears that a mapping radar with a resolution of approximately 30 m will be in demand for airborne remote-sensing applications, particularly in the Earth-science fields.

A 30-m resolution requirement is not readily obtainable from an RAR. However, a cost-effective approach to this requirement is available that will retain the advantageous features of the RAR. This approach uses synthetic aperture processing and is known as a coherent-on-receive radar.

Resolution is not the only criterion used in selecting an airborne remote-sensing radar. Much work has been done in recent years on the detection and classification of terrain features by multifrequency and multipolarization measuring techniques. These techniques, which will not be discussed in this section, may be applicable to all SLAR systems, depending on the particular remote-sensing problem.

Basic Principles

Radar mapping systems depend on the principles (1) that all material reflects a portion of the electromagnetic energy radiated on it, and (2) that electromagnetic energy travels in straight lines and at constant velocities. Energy directed from an antenna in a beam is reflected from the ground, which can be considered as an extended array of scatterers. A radar map is obtained by scanning the ground and displaying the amplitude-modulated returns on a cathode-ray tube (CRT) or photographic film. The magnitude of ground reflections depends in a complex way on such factors as incident angle, target size and shape, material properties, and so forth. In general, a larger sur-

face reflects more radar-transmitted energy than a small surface. Strongest reflections usually occur when the radar beam arrives at right angles to the reflecting surface. Certain materials are better reflectors than others. Of the commonly used structural materials, wood is the poorest reflector, whereas steel is the best reflector. Masonry without metal reinforcement is a fair reflector. Lakes, rivers, runways, or similar smooth, horizontal terrain features reflect radar signals as a flat mirror reflects a beam of light. Little of the radiated energy that strikes this type of terrain, at low grazing angles, is reflected back to the radar receiver.

The SLAR often produces photoradar maps of the terrain on one or both sides of the aircraft flightpath. The SLAR differs from other scanning radar systems in that the antenna is fixed to the aircraft, and its radiation pattern is perpendicular to the groundtrack. Scanning the area is accomplished only by the movement of the aircraft in flight.

The SLAR systems use an antenna beam pattern having a very narrow dimension in the horizontal direction and having wide angular coverage in the vertical direction, thus illuminating a long narrow strip of ground from beneath the aircraft to some maximum range. Therefore, the antenna beam illuminates the ground at many different ranges and incident angles. If not corrected, this condition would make correlating the strength of the radar returns with actual terrain features very difficult.

To compensate for the effects of range, the vertical gain pattern of the radar antenna is designed to be a function of the slant range or incident angle at which a given ground-patch is viewed. This type of antenna pattern is commonly called a cosecant-squared beam. At one altitude and assuming flat terrain of homogeneous properties, the radar returns from all ranges out to a maximum could theoretically be made equal. Practically, this condition can be attained only within some tolerance (usually ± 2 dB) over a limited range of vertical angles. Changes in

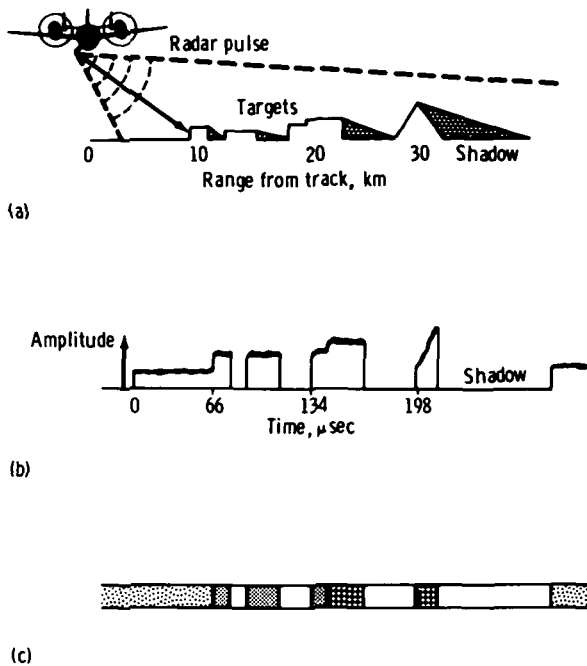


FIGURE 5-11.—Simplified representation of SLAR image recording. (a) Targets and shadow effect. (b) Radar return echoes. (c) Intensity of CRT trace.

ranges, the capability is called an unfocused SAR. Usually, this processing is accomplished on the ground after a flight by using an optical correlator. Recently, work has been performed on digital correlators that can operate on a real-time basis in the air. Optical correlators of the required quality are not suitable for aircraft installation, primarily because of their bulk.

The SAR systems usually incorporate chirp techniques to obtain high range resolution without requiring excessively high peak power transmitters. A coherent signal is required to generate chirp signals and to form a synthetic beam. Generally, such systems use a stable local oscillator (STALO) to generate the transmitted signal and to serve as a local oscillator in the receiver. A pulsed power amplifier is used to produce the high power transmitted signals.

Important System Considerations

The selection of an SLAR for remote sensing requires that certain key perform-

ance parameters be evaluated by the user. The user must understand the performance and cost tradeoffs so that a cost-effective selection can be made. Some of the more important characteristics that should be considered are presented in the following paragraphs.

Resolution.—A key parameter often used to judge the quality of mapping radar is resolution. With SLAR, resolution is defined as the minimum separation between two targets that will appear individually on the imagery. Whereas the ultimate system resolution is a function of several parameters, the most important criterion is the size of the radar pulse rectangle projected on the ground. At a given instant of time, the ground area (ΔR by ΔY) is simultaneously superimposed in the radar receiver (fig. 5-12). This area is called the pulse-rectangle or ground-resolvable area. Objects within the pulse rectangle are recorded as if they were all located at the center of the rectangle, and two objects that occupy the same pulse rectangle appear as a single return on the imagery. The integrated reflectance of all ground area and of all objects within the ground-resolvable area at any given instant are, in essence, presented as one value of reflectance to the sensor. When this composite reflectance value differs from those in adjacent pulse rectangles, the sensor can discriminate between targets. If a single "hard" target (such as a small truck) is in flat, open surroundings and is illuminated by the radar, it probably will be the dominant reflector in the pulse rectangle. The radar accordingly records, as a single target, the composite reflectance of the truck and the surrounding area within the pulse rectangle. To the radar, the truck is as large as the ground-resolvable area. If objects are separated by a distance greater than the corresponding dimension of the pulse rectangle, they will be imaged separately.

One should be careful to distinguish the difference between detection and resolution associated with a mapping radar. Resolution is commonly defined as the ability of the

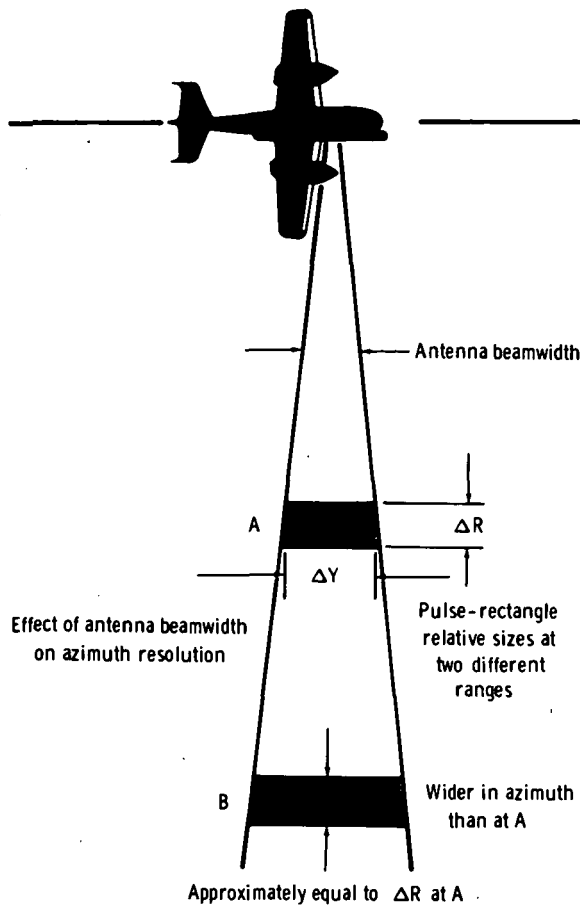


FIGURE 5-12.—Real aperture resolution.

radar to distinguish two targets of equal reflectivity separated by the resolution distance. However, this definition does not imply that the radar cannot detect a target smaller than the resolution cell. If a target has sufficient reflectivity, the radar will detect a target, such as a vehicle, a powerline pole, a corner reflector, and so forth, even though it may be physically much smaller than the resolution cell of the radar. Because of this difference in detection and resolution, users of RAR are often amazed by the detail in the imagery, because of the many small features that are detected when resolution is not required to distinguish them from surrounding objects.

For real aperture noncoherent SLAR, the pulse rectangle (ground-resolvable area) is

primarily determined by the radar antenna beamwidth and transmitted pulse length. Range resolution, which is in the direction of radiated energy (perpendicular to the flightpath), is determined by the bandwidth of the transmitted signal. The inherent range resolution $c\tau/2$ is transformed into ground resolution by

$$\Delta R = \frac{c\tau}{2 \cos \psi} \quad (5-4)$$

where ΔR is ground range resolution, τ is transmitted pulse width (3 dB), ψ is beam depression angle, and c is speed of light. For an RAR and small horizontal antenna beams, the azimuth resolution is a function of half-power beamwidth $\theta_{-3 \text{ dB}}$.

$$\theta_{-3 \text{ dB}} = \frac{K\lambda}{D} \quad (5-5)$$

where K is efficiency factor of antenna aperture, λ is transmitted wavelength, and D is antenna aperture length. The azimuth resolution ΔY is given by

$$\Delta Y = R\theta_{-3 \text{ dB}} = \frac{RK\lambda}{D} \quad (5-6)$$

where R is range.

Azimuth resolution can be improved by decreasing the wavelength λ (increasing frequency) or by increasing the physical dimension of the antenna. Either approach has a limit in a practical radar design. In decreasing the wavelength λ , the problems of atmospheric attenuation and the efficient generation of large amounts of power become more difficult. The problems of an excessively large antenna are quite obvious when considering airborne or spacecraft installations.

For the unfocused synthetic array for which no adjustments are made in the return-signal phases before integration, there is a limit to the effective synthetic antenna length that can be generated. The criterion often used is that the difference between the round-trip distance from the target to the center of the array and the round-trip distance from the target to the extremity of the array should not differ by more than $\lambda/4$ (fig. 5-13).

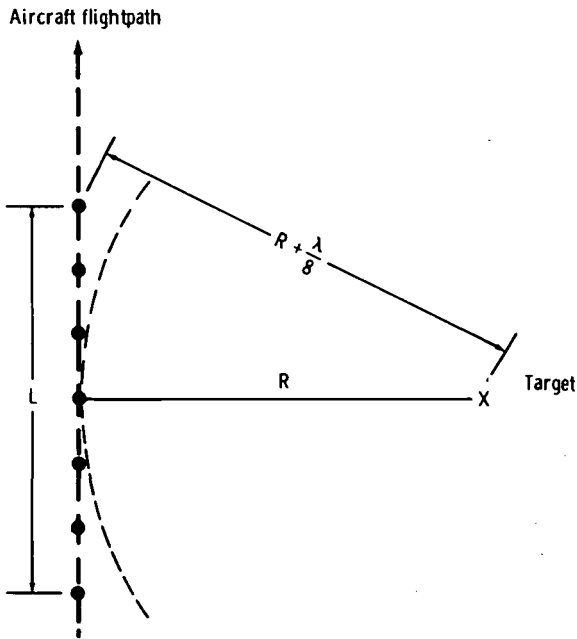


FIGURE 5-13.—Unfocused synthetic antenna.

When this rule is used, the best azimuth resolution obtainable from an unfocused radar is

$$\Delta Y_u = \frac{1}{2} \sqrt{\lambda R} \quad (5-7)$$

Although range is still an important criterion, it is less important with the unfocused synthetic array than with the RAR. More importantly, the azimuth resolution at long ranges is not a function of the physical antenna length D .

If the radar processor makes adjustments in the signal phase received at each point of the synthetic antenna (focusing), the restrictions that limited the maximum synthetic antenna length of the unfocused antenna no longer apply. The best obtainable azimuth resolution from the focused SAR is

$$\Delta Y_f = \frac{D}{2} \quad (5-8)$$

The smaller the physical aperture, the wider the physical beamwidth; and, consequently, the longer the portion of the flightpath during which the returns of a given target can be processed to form the synthetic aperture.

This expression also forms the limit at short ranges for the azimuth resolution of the unfocused processor.

Distortion.—Image distortion is as important, in many respects, as system resolution. A distorted image makes it difficult to make the proper interpretation of actual terrain features. Although there are many sources, the types of distortion errors that should be given special consideration are azimuth resolution distortion, display distortion, and antenna motion distortion.

In the discussion of resolution, the pulse rectangle of the RAR was shown to grow in azimuth direction as the target range was increased (fig. 5-12). As a result, objects that are approximately equal in range and azimuth dimensions will be shown to be extended in azimuth, relative to range. This fact also obtains for targets mapped by an unfocused SAR, but to a lesser degree because azimuth dimensional relationships remain constant for focused SAR.

Display distortion can result from several factors, including nonlinear sweeps and improperly designed optics. However, most errors of this type can be minimized by proper hardware design. Skew distortion of the image will occur if no compensation is made for aircraft drift and antenna squint angle. If a slant-range presentation is used, a foreshortening of targets at close range will occur. When ground range is displayed based on assumed level terrain, the image will be distorted if the terrain is sloping or irregular. If the antenna is rigidly fixed to the aircraft, buffeting and turbulence may smear and distort the radar image.

If the antenna pattern is not continually positioned perpendicular to the aircraft groundtrack, some form of correction must be provided to prevent square objects from being recorded as skewed parallelograms and circular objects from becoming elliptical. Generally, this skew distortion is corrected by yaw stabilization of the antenna and by providing drift information from the navigation system to the deflection yoke of the CRT. The true direction of the antenna beam is not

necessarily perpendicular to the face of the antenna array. The deviation of the beam from the orthogonal is called the squint angle. If the CRT traces are rotated an amount equal to the sum of drift and squint angle and expanded by the cosecant of the sum angle, the radar image will be free from skew distortion and range error.

Some radars display slant range from the aircraft to the target, which is reasonably accurate for small depression angles but causes close-in targets to appear farther away than the true distance from the aircraft groundtrack. The close-in distortion can be improved by a nonlinear sweep signal on the CRT, making the map dimensions proportional to true ground range. However, the aircraft altitude above some reference plane must be accurately known. This reference plane is normally measured with respect to the terrain directly below the aircraft flightpath. If the topography is highly irregular or sloping, range errors will still exist for all target areas not located on the reference plane.

For a radar system to generate high-quality photoradar maps, the aircraft should move over the ground at a constant velocity and maintain a stable attitude with respect to the ground. If the attitude of the aircraft varies, the movements may have adverse effects on the radar image. Roll, pitch, and yaw motions may be due to meteorological variables and autopilot discrepancies caused by improper operation or malfunction.

For RAR, the degree and precision of motion compensation or stabilization is relatively minor. Stabilization of the antenna about the yaw axis to within a beamwidth is generally all that is required for good-quality RAR imagery.

Stabilization of the antenna is a vitally important factor for high-resolution SAR. A greater degree of motion stabilization and correction is required as the resolution requirement becomes more extreme. Turbulent aircraft motion along the flightpath can "bend" or distort the synthetic antenna return. Generation of a high-resolution map

is based on accurate determination of phases and Doppler frequencies of the return signal. If motion errors are not detected and appropriate corrections are not made, the map quality will be degraded to an unacceptable degree. Usually, the antenna is stabilized by a system of roll, pitch, and yaw gimbal drives that are controlled from signals generated in a motion compensation subsystem of the radar.

Range coverage and swath width.—For remote-sensing applications, range coverage and swath width are very important considerations that have a direct influence on the total cost effectiveness of any radar mapping mission. A radar with greater range coverage and swath width will undoubtedly result in lower operational cost, and will require less time, equipment, and manpower. This cost reduction is extremely important in commercial remote sensing.

For real aperture mapping radars that use the analog signal integration of the CRT and film, the maximum mapping range is limited primarily by transmitter power, antenna aperture size, and atmospheric attenuation. When digital processing is used, the overall complexity and cost of the processor may impose some practical restraints on swath width. The rapid development of LSI (large-scale integration) integrated circuits is making the use of real-time digital processing more attractive.

Real aperture X-band mapping radars that cover as much as a 200-km swath width are now in production. Usually, the SAR is limited to smaller swath widths (15 to 30 km) because of hardware complexity and transmitter power limitations.

All-weather capability.—In an RAR system with a fixed antenna size, the azimuth resolution is improved in proportion to the frequency of the transmitter. For this reason, designers use the highest transmitter frequency that also has other acceptable characteristics, such as low atmospheric attenuation. The X-band is a reasonable compromise between achieving high resolution and selecting a frequency with desirable propagation

characteristics. The X-band is the highest microwave frequency range that has acceptable low attenuation and backscattering properties through cloud cover and moderate rainfall. A real or unfocused SAR operating at Ka-band would provide better azimuth resolution for a given antenna length, but at the price of increased propagation losses and severely limited performance in weather conditions in which water droplets are formed.

Another important advantage of radar for geological survey applications is the ability of this type sensor to provide some penetration of foliage to reveal the rock formations below. In vegetated areas, the X-band radar imagery has revealed faultlines that were not detectable in photoimagery, even though relatively little foliage penetration is obtained at X-band. A lower transmitter frequency (e.g., 400 MHz) would provide much better foliage penetration, but the loss in azimuth resolution for an RAR makes this impractical. The SAR could provide good resolution and some foliage penetration by operating at these lower frequencies.

Availability of data.—The timeliness or turnaround time required for radar data is primarily a function of the mission objectives. When the terrain being mapped is static or slowly changing, such as mountain ranges or agricultural areas, it might appear that real-time data are not required. However, this is not the case. For example, when mapping an area to detect geological features (such as faults, fractures, and minor topographical features), the correct amount of shadowing must be produced on the map. The proper degree of shadowing will enhance the topography, whereas too much or too little shadowing will result in lost information. An airborne operator able to view imagery during flight can optimize the shadows by adjusting the flight altitude.

When the terrain is in a state of continual change, such as in ice-field mapping or oil pollution detection, a large time delay in transmitting the information to a ground station where it is processed, interpreted, and

disseminated to the using agencies may be unacceptable.

When large areas are to be surveyed, it is practical to construct map mosaics from adjacent strips of radar imagery. Good-quality mosaics require that the overlap of each strip be properly controlled and that the amount and direction of the image shadows be the same for each strip. Real-time monitoring of the radar data by a qualified operator is vital to producing good-quality mosaics.

Real-time film developing for current SLAR systems is accomplished by onboard film-processing laboratories in the larger aircraft systems or by self-contained monobath-processing cameras. With the latter approach, exposed film passes under a metering roller at which time it comes into contact with chemical-processing fluid. Processing fluid is vacuum pumped from a sealed monobath tank into a processing tray and returned to the tank. After the film has been processed, it moves into view over a lighted viewing panel, which presents ground targets in the viewing area a few seconds after the area is illuminated by the radar.

Real Aperture SLAR Applications

This section briefly describes some environmental and geological applications of SLAR. Although these applications are not a complete listing, they give some indication of the versatility of SLAR as a remote sensor.

Oil and mineral exploration.—The usefulness of SLAR in locating gas and oil fields and mineral deposits lies in the ability of the radar to provide a large-area map, which enables surface lineaments to be detected. Analysis of the density and directional distribution of surface lineaments can isolate oil- and gas-bearing subsurface structures. This detailed radar lineament analysis is possible because the radar provides an image that enhances the geological features better than conventional aerial photography. The SLAR has the unique capability of operating with a wide selection of depression angles, which allows the operator to enhance the topographic features in areas of high or low relief.

An example of the imagery produced is shown in figures 5-14 and 5-15, which illustrate some of the features of the AN/APS-94D SLAR. The wide-area surveillance capability of a real aperture SLAR is demonstrated in figure 5-14. Swath width on this image is 100 km (50 km on each side of the aircraft flightpath). The enhancement of geographical features by SLAR is shown in figure 5-15.

Another advantage of SLAR for geological exploration is the ability to image simultaneously from both sides of the aircraft to facilitate making two radar mosaics of the terrain with opposite look directions. Thus, the imagery interpreter is better able to locate less-pronounced lines or fractures that might not be visible from a particular look direction.

The SLAR does not, of course, provide complete knowledge of geological features;

however, it provides much information that permits surface exploration to be concentrated in areas with the highest probability of success.

Ice mapping and classification.—The SLAR imagery provides information on the amount and nature of ice cover for either saltwater or freshwater areas. The principles of operation are somewhat different from the mapping of ground areas because ice, under certain conditions, appears transparent to the microwave energy and does not reflect energy to indicate its presence. Thus, ice imagery requires careful interpretation. Different types and amounts of ice cover are illustrated in figure 5-16. The bright lines and areas in the image represent the points of greatest radar echo. The echoes result primarily from interface between ice and water or discontinuities or cracks in the ice that are nearly perpendicular to the line of sight. The pres-

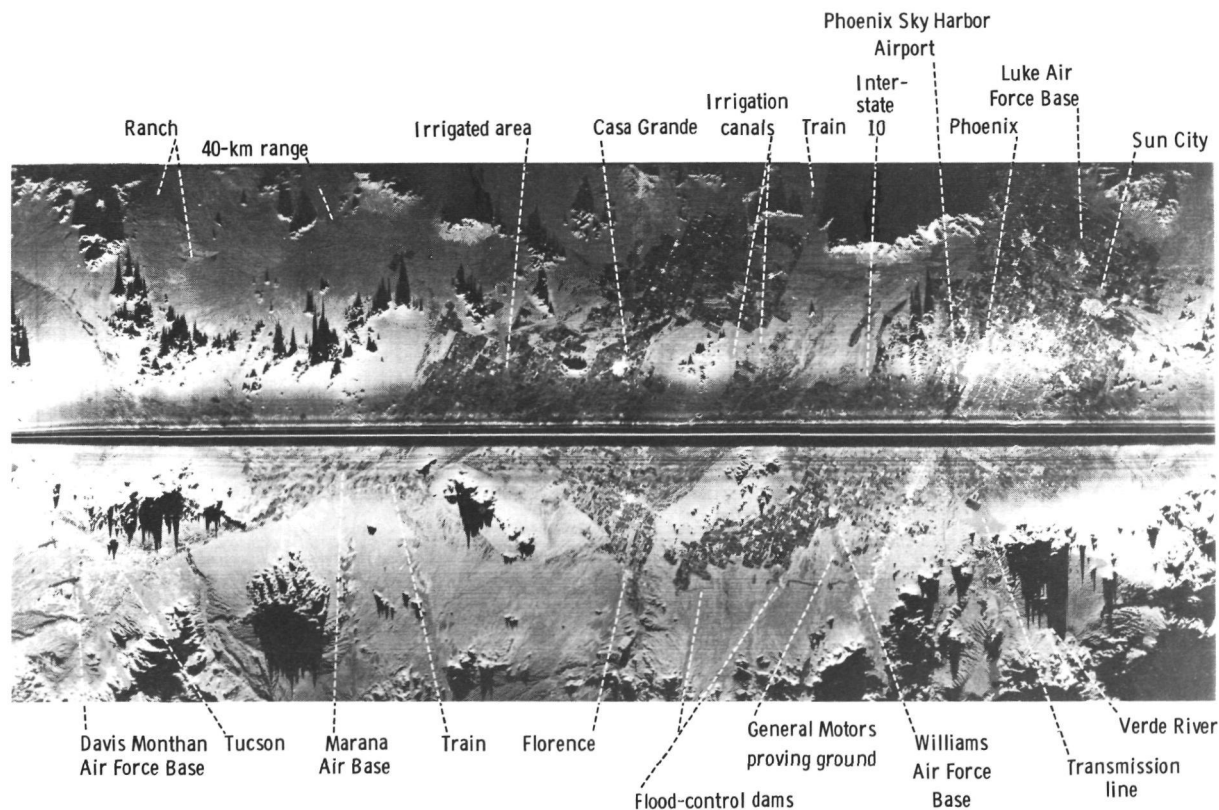


FIGURE 5-14.—Wide-area surveillance capability of a real aperture SLAR (AN/APS-94D fixed-target imagery of central Arizona).

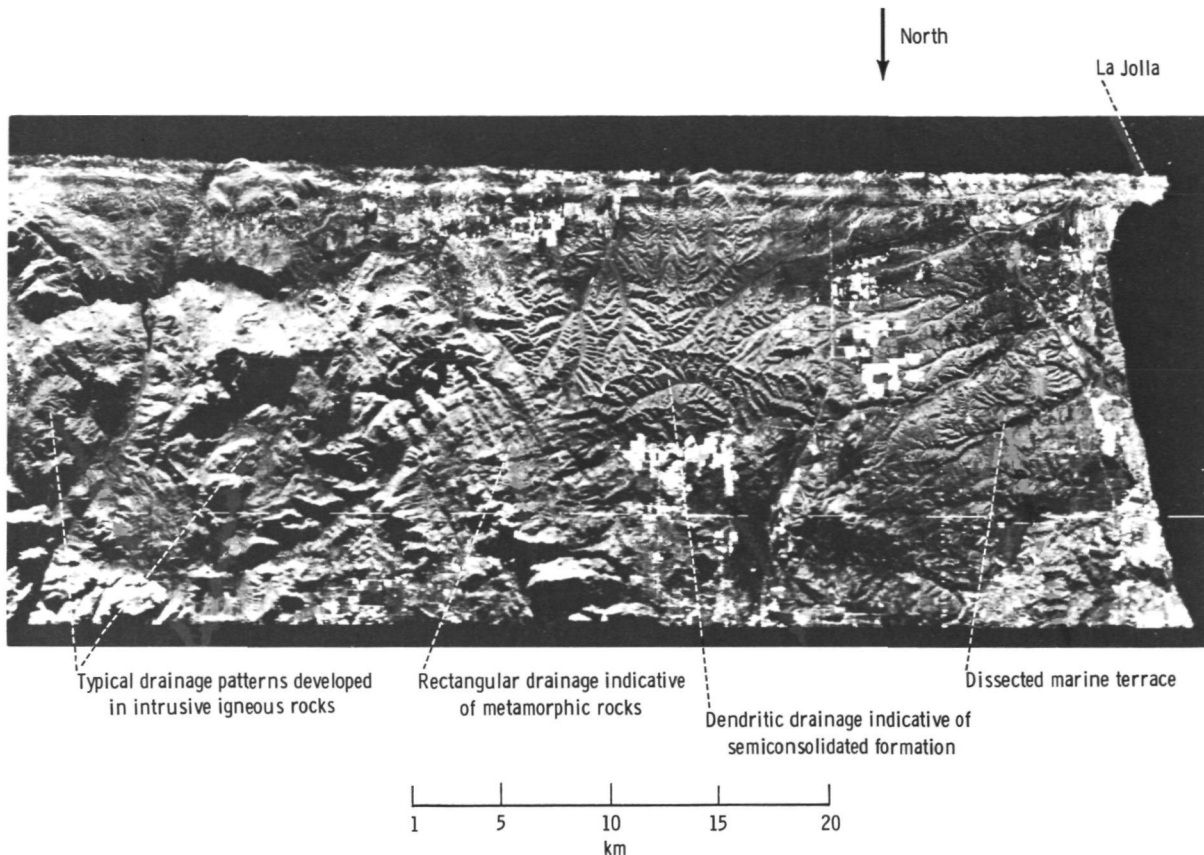


FIGURE 5-15.—Enhancement of geographical features by SLAR (AN/APS-94D fixed-target imagery of La Jolla, Calif., with a 25-km range and a single antenna).

ence of clear ice in the upper portion of figure 5-16 is primarily evidenced by the presence of pressure ridges and cracks. The clear area in the left portion of figure 5-16 shows the greatest amount of radar reflection and indicates the turbulent flow of ice in that area. The interpreter's ability to determine the nature of the ice cover is aided by knowledge of other meteorological conditions, such as the temperature, force, and direction of the surface wind.

The ability of SLAR to produce imagery through cloud cover and surface storms is particularly important because the information is of greatest value during these conditions. A radar operating at a wavelength of approximately 3 cm can penetrate cloud cover that would prevent visible and infrared (IR) sensors from producing ice imagery.

Icepack tracking.—The location of ice-

packs and icebergs is of prime importance to surface vessels in the area. The best information on the movement of these hazards is obtained by periodic mapping of the area with side-looking radar. The movement of ice on the water is governed by both winds and tides. Present experience indicates that the location can be determined accurately enough to permit safe passage of surface ships if an SLAR map can be obtained every few days. The required frequency of reconnaissance flights depends on the wind conditions and the particular areas involved. Attempts to predict the movement of ice by the speed and direction at the time of reconnaissance would not be useful because of the erratic nature of the movement and the inability to measure low velocities with a high degree of accuracy.

The ability of the SLAR to produce a

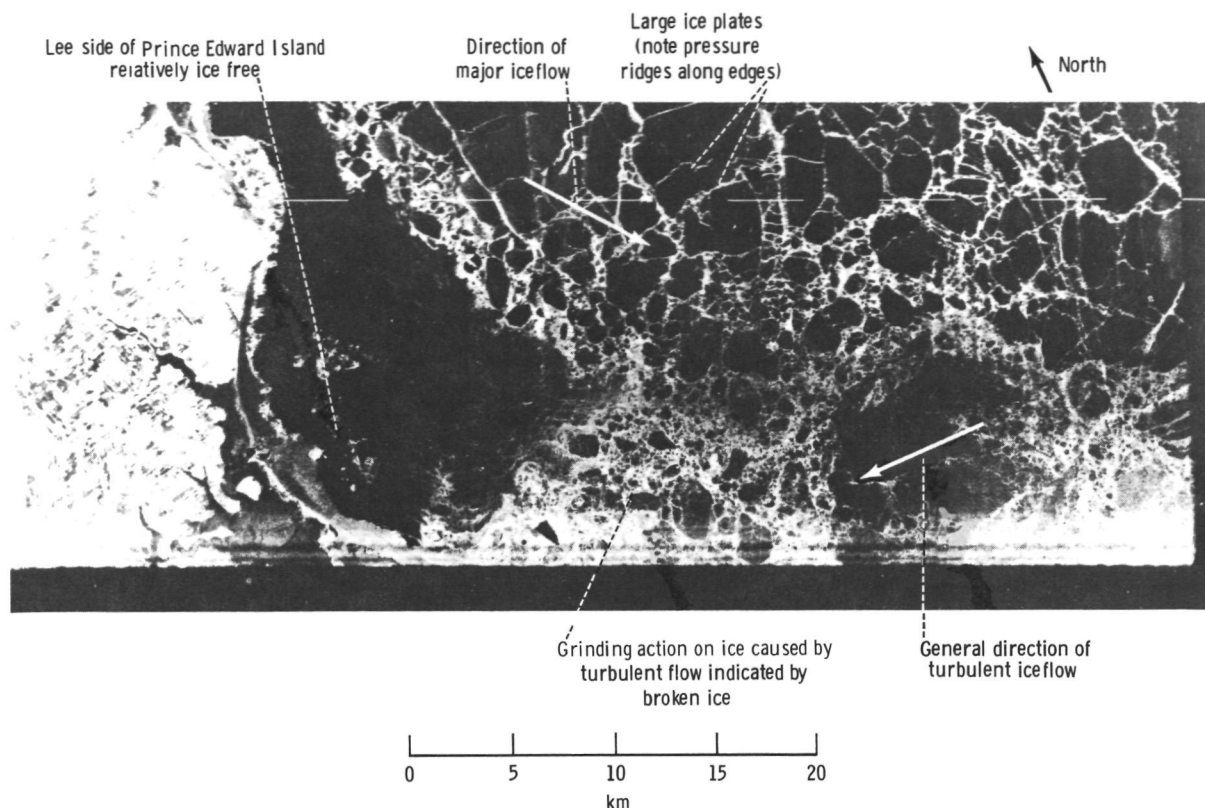


FIGURE 5-16.—The SLAR imagery of varying types and amounts of ice cover (AN/APS-94D fixed-target imagery of the northwest tip of Prince Edward Island).

200-km-wide radar map under adverse weather conditions is again a great advantage. Because icebergs produce large radar echoes, resolution is not of particular importance, and the radar can be operated on the largest scale factor and greatest range.

Oil pollution detection.—With the ever-increasing demand worldwide for crude oil and petroleum products, accidental spills from ships and offshore wells are becoming an increasing danger. To combat this potential hazard, the U.S. Coast Guard has developed an Airborne Oil Surveillance System (AOSS). The AOSS is a multisensor system consisting of an X-band side-looking radar, a Ka-band imaging microwave radiometer, a multichannel IR line scanner, and a multispectral low-light-level (LLL) television (TV) system. The AOSS is designed to detect and map oilspills anywhere within a

40-km range of the aircraft flightpath. The system was flight tested in early 1974. The following are functions of the AOSS:

1. To detect oilspills on the sea.
2. To indicate the magnitude of oilspills (both area and approximate thickness).
3. To assess cleanup operations and forecast dangers to coastal areas.
4. To identify the oil type (signature).

This set of complex requirements cannot be satisfied by a single sensor; thus, the AOSS combines microwave techniques and other methods using radiation from the ultraviolet to the IR region. The mission concept is depicted in figures 5-17 and 5-18.

The side-looking radar will provide long-range routine surveillance of an area as much as 40 km on each side of the aircraft. The microwave radiometer covers the area directly below the aircraft flightpath (not

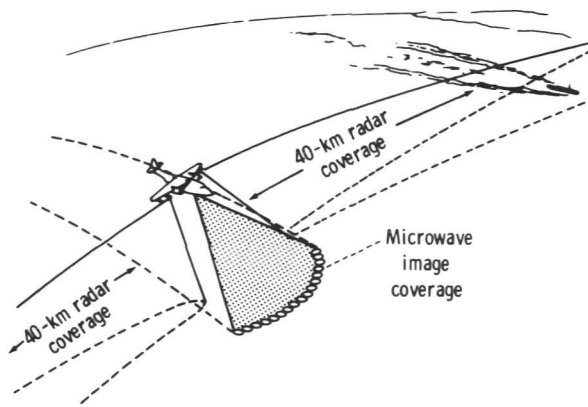


FIGURE 5-17.—Routine AOSS surveillance at a 1524-m altitude (ship detection and routine ocean slick mapping mode).

mapped by the radar). The radar imagery provides the location and approximate area of the oilspill, and once the oilspill has been identified, a short-range inspection is made by other sensors that classify and measure characteristics of the oilslick.

The active microwave sensor advantageously uses contrast in reflection properties between clean and polluted seas. Small-amplitude waves of short length are continually generated on both calm and high seas. These waves are efficient reflecting surfaces for microwave radiation. A thin

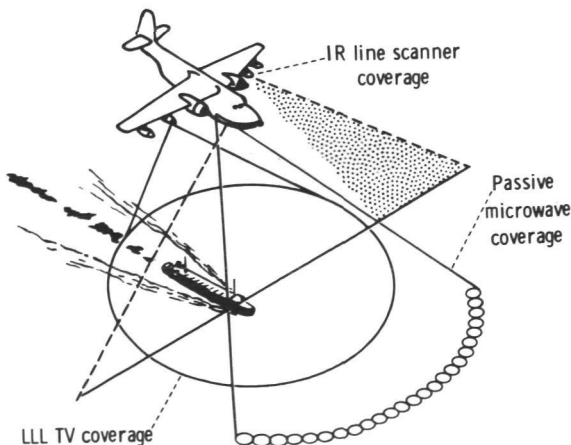


FIGURE 5-18.—Diagram of AOSS short-range pollution inspection and documentation (low-altitude ship and pollution inspection and documentation mode).

film of oil damps these small gravity and capillary waves, forming a surface of lower radar reflectivity. Active microwave sensors can easily detect the change in microwave reflectivity caused by oil, except in the presence of very calm sea states (with prevailing winds less than approximately 1 m/sec). A summary of other requirements for the radar used on the AOSS is given in table 5-IV.

Tradeoff Considerations

The basic principles of an SLAR sensor have been examined, and some of the important considerations in the system design have been reviewed. In summary, the significant desirable features of an SLAR sensor are long-range coverage, broad swath width, adequate resolution and detection capability, all-weather operation, in-flight processing and imagery viewing, reliable design approach, moderate system acquisition costs, and low operational costs.

Although real-time film processing that uses wet chemical developing is available, a dry-film-processing camera would be a definite improvement in terms of operational costs and handling problems.

The most direct approach to improving azimuth resolution in RAR is to extend the physical length of the antenna. However, improved resolution is obtained at the expense of additional atmospheric and weather attenuation effects. When improved azimuth resolution is required, some type of synthetic processing technique can be used, but careful

TABLE 5-IV.—Requirements for Radar Used on AOSS

Range:	
Ship detection, km....	0 to 40
Oil spill detection, km.	15 to 25
Swath width, km.....	80
Detection requirements	
Ships, m	≥ 25 by 80 (or larger)
Large spills (major dimension), km....	> 1.5
False alarm rate, max/hr..	1
Data	Hardcopy (film)

thought should be given to how much resolution is required to accomplish the task.

Resolution tradeoff considerations.—A tradeoff between SAR and RAR can only be made when the specific application of the radar is considered. For many environmental applications, such as geological fault surveys, geological exploration, ice reconnaissance, and water-level surveys, large-area moderate-detail imagery is required. The initial purchase cost, maintenance cost, and total mission operating cost of a high-resolution SAR is not justified solely for these applications. The greater swath-width coverage of the real aperture system more than offsets the lower resolution associated with this type of airborne radar. Usually, wide-range swath width and high resolution are incompatible because of practical limitations on the complexity of processing and recording equipment.

If fine topographical detail is required to obtain the desired target intelligence, the high-resolution SAR has an advantage. Some possible applications might include land use and urban studies. Again, the specific applications of the radar system may indicate whether the need to resolve the fine detail occurs frequently enough to justify a high-resolution radar.

An aircraft system used for environmental applications probably will contain multispectral sensors such as optical, IR, microwave, and magnetic sensors. In such instances, the most cost-effective system might include a side-looking radar for rapid large-area coverage. The SLAR provides gross detail and draws attention to probable areas in which closeup, highly detailed data are required.

Alternate approaches to synthetic aperture processing.—As an aid to selecting a cost-effective system, the azimuth resolution obtainable from various approaches will be reviewed.

For RAR, the best obtainable azimuth resolution is

$$\Delta Y_r = \frac{\lambda R_s}{D} \quad (5-9)$$

For an unfocused SAR, the azimuth resolution is

$$\Delta Y_u = \frac{1}{2} \sqrt{\lambda R_s} \quad (5-10)$$

Finally, the fully focused SAR azimuth resolution is

$$\Delta Y_f = \frac{D}{2} \quad (5-11)$$

where λ is wavelength, D is effective antenna real aperture length, and R_s is slant range. The preceding expressions represent the resolution obtainable in an ideal system. In actual system designs, the overall resolution may be somewhat less than these predicted values. A graphic comparison of the theoretical resolution obtainable when λ is 3.2 cm and D is 3 m is shown in figure 5-19. Note that for a focused synthetic processor, resolution can be improved by decreasing the antenna length D (curve D in fig. 5-19). The unfocused example (curve C in fig. 5-19) assumes a uniformly weighted filter with

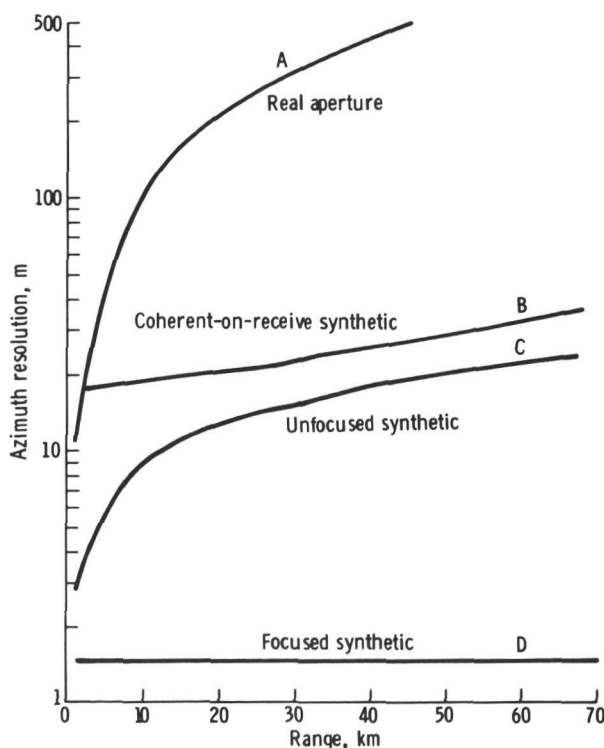


FIGURE 5-19.—Ideal azimuth resolution as a function of range, where λ equals 3.2 cm and D equals 3 m.

bandwidth varying as a function of the square root of range. A more practical design approach might use a Taylor weighting to minimize side lobes and a fixed bandwidth (curve *B* in fig. 5-19).

Cost tradeoff considerations.—Although precise cost comparisons are difficult to make, no system concept can be selected without some rough estimate of the overall cost, including both the airborne sensor and ground-processing equipment. It is fairly safe to state that system acquisition costs are heavily influenced by the resolution requirements. The RAR systems are the least expensive, and the focused synthetic radar is, of course, at the high end of the cost scale. The relative cost of X-band SLAR as a function of azimuth resolution is illustrated in figure 5-20.

Recommended future system developments.—Because of the wide diversity of requirements, no single SLAR design will meet all remote-sensing requirements in a cost-effective manner. In some applications, the RAR will be adequate; in others, state-of-the-art synthetic radars with multiple frequency and multiple polarization may be needed. However, for the vast majority of remote-sensing problems, a radar with moderate resolution (30 m) appears to be adequate. For these problems, an X-band unfocused synthetic aperture or Doppler-beam-sharpened design

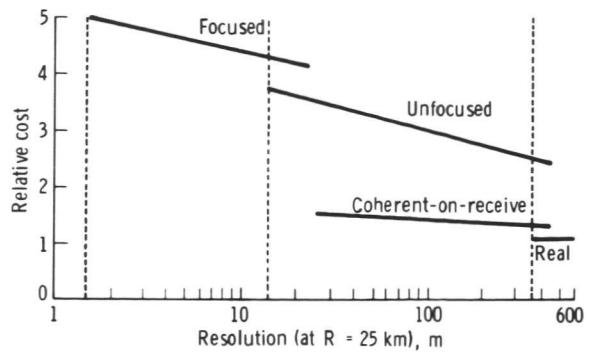


FIGURE 5-20.—Relative cost of X-band SLAR as a function of azimuth resolution.

approach is recommended. There is nothing really new about the basic concept of Doppler beam sharpening; in fact, such radars are now in existence. However, the design approach briefly described in the following paragraphs represents a lower cost alternative to the fully coherent unfocused synthetic radar design. Some tradeoffs considered in selecting the coherent-on-receive approach are summarized in table 5-V.

A list of key performance characteristics of a mapping radar that should satisfy numerous remote-sensing applications during the next 5- to 10-yr period is given in table 5-VI. This radar is primarily intended for remote-sensing problems that require moderate resolution.

TABLE 5-V.—Summary of Tradeoff Considerations

Performance improvement	Recommended method	Alternate method	Reasons for not selecting alternate
Range resolution . . .	Short transmitter pulse.	Pulse compression.	Klystron or traveling-wave tube must be used instead of a simple, inexpensive magnetron transmitter.
Azimuth resolution . .	Coherent-on-receive synthetic aperture.	Increase frequency of RAR.	Range decrease is caused by atmospheric losses, and more expensive microwave components are needed.
		Increase antenna length of RAR.	Antennas 5 m or less can be carried by business aircraft, whereas larger antennas would require transport-size aircraft.
		Fully coherent synthetic aperture.	Although the fully coherent design has highest ultimate resolution potential, the coherent-on-receive design provides an order-of-magnitude improvement over real aperture and retains magnetron transmitter.

TABLE 5-VI.—*Coherent-on-Receive Radar Parameters*

Transmitter:	
Tube type	Magnetron
Frequency	X-band
Peak power output, kW.	50
PRF, pulse/sec	750
Pulse width, μ sec.....	0.2
Receiver:	
Minimum discernible signal, dBm	-95
Bandwidth, MHz	7
Antenna:	
Gain, dB	35
Elevation pattern shape.	$\csc^2 \theta$
Stabilization	Yaw plane
Antenna length, m.....	3
Polarization	Horizontal
Look direction	Both sides of aircraft
Processor type	Unfocused synthetic coherent-on-receive
Range resolution, m.....	30
Azimuth resolution (at 25 km), m.....	30
Range scale, km.....	25 or 50
Maximum swath width, km..	100
Data display	Real-time using dry silver film recorder

Coherent-on-Receive System

In a coherent radar system, the echo is processed to extract both amplitude and phase information, as opposed to a noncoherent radar system in which only amplitude information is processed. A coherent system will generally produce far better performance than a comparable noncoherent system. There are two basic approaches for achieving coherent operation. The most commonly used approach (i.e., the fully coherent system) uses a STALO and a power amplifier transmitter. Each transmitted rf phase is locked to the STALO, which is required to have very limited phase and frequency variations during the observation time of any representative target.

The coherent-on-receive technique is a method for generating a coherent signal from a magnetron transmitter. The phase of a magnetron transmitter will be approximately random from pulse to pulse. Coherence is obtained by measuring the phase of the echo

from that pulse. Removal of the transmitted phase from the echo phase eliminates the random pulse-to-pulse phase variations so that the signal may be processed as a coherent signal. Thus, the signal is not coherent until it is received by the radar and the random phase error is removed.

The coherent-on-receive operation is generally not economical in systems requiring modulation, or chirp, of the transmitted phase. Such intrapulse modulation is generally required only when the desired range resolution of a mapping radar is high. The desired range resolution is available by transmitting a fairly short pulse (0.1 to 0.2 μ sec), which is still long enough for practical peak-power considerations.

The key element of the coherent-on-receive radar is the measurement of the phase of each transmitted pulse and the subtraction of that phase from the subsequent echo train. The significant steps in accomplishing this operation are summarized as follows:

1. At the time of transmission, a sample of the transmitter is injected into the receiver (fig. 5-21).
2. The phase angle θ_t of the transmitted signal is measured in the receiver and stored.
3. The phase angle θ_e corresponding to the transmitter phase is subtracted from the echo signal phase history that resulted from the transmitted pulse.
4. This operation is repeated for each radar-transmitted pulse.
5. The echo signal pulse train can now be processed as a pulse-to-pulse coherent signal.

Any errors in the magnetron, the STALO, or the intermediate frequency will be converted into phase errors by the phase-measurement circuit. These sources of frequency errors must be minimized to keep the resulting phase error within acceptable limits.

Antenna.—Because the coherent-on-receive radar is a variation on the unfocused synthetic aperture technique, the physical aperture of the antenna does not affect the system azimuth resolution. The major considerations that determine the antenna size are (1) gain adequate to provide the desired

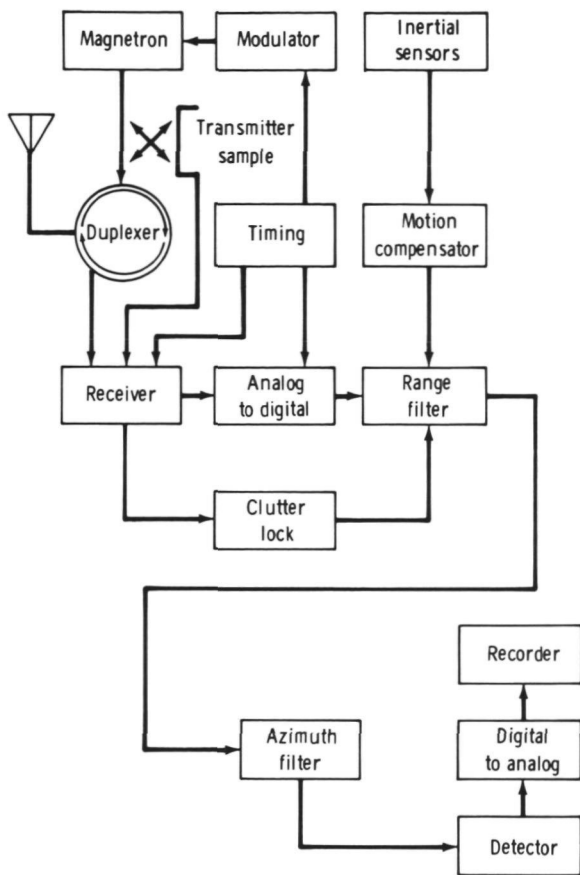


FIGURE 5-21.—Simplified block diagram of coherent-on-receive SLAR.

operating range, and (2) size small enough for convenient installation on a medium-sized aircraft.

A 3-m X-band phased-array antenna will have less than a 1° beamwidth (3 dB) in the azimuth plane. If the elevation pattern has a cosecant-squared shape, the peak antenna gain will be approximately 35 dB.

The optimum polarization depends on the intended remote-sensing application. For example, for oilslick detection, vertical polarization would be best, but horizontal polarization is optimum for geological survey work. An antenna with selectable polarization would solve both problems if the added cost can be justified. Horizontal is probably the best selection if only one linear polarization is to be used.

Receiver/transmitter.—The receiver/transmitter has all the elements of a standard noncoherent radar. The major differences include a local oscillator that has greatly improved frequency stability, and a sample of the transmitted pulse is summed into the receiver. These modifications make it possible to compare the relative phase of the transmitted signal and the received echo on a pulse-to-pulse basis. Typical characteristics of the receiver/transmitter are given in table 5-VII.

The stability requirements for the local oscillator for this system are more stringent than for noncoherent radar. The local oscillator consists of a highly stable crystal oscillator and a multiplier chain to obtain the X-band output. The basic frequency is chosen to obtain the best short-term frequency stability. The oscillator has a short-term stability of 1 part in 10^{10} when averaged over a 1-sec period.

Processor.—A simplified block diagram of a Doppler-beam-sharpened fixed-target processor is shown in figure 5-21. The video data are sampled by the analog-to-digital (A/D) converter and converted to digital numbers or words. Following the A/D conversion, a buffer stores data at the conversion rate of the A/D converter and writes out the data at a slower rate to fill the interpulse period completely.

The range filter removes the spectral offset frequency and divides the signal into in-pulse and quadrature channels, with each channel operating at half the input data rate. This result is achieved by first multiplying the signal by $\exp(-j\omega_0 t)$, where ω_0 is the signal offset frequency. This multiplication shifts the spectrum to zero, but it also produces an

TABLE 5-VII.—Typical Characteristics of the Receiver/Transmitter

Peak power output, kW.....	50
PRF, pulse/sec	750
Pulse width, μ sec.....	0.2
Minimum discernible signal, dBm.....	-95
Receiver bandwidth, MHz.....	7

undesirable spectrum centered about $2\omega_0$. A low-pass-filter operation eliminates the spectrum centered at $2\omega_0$. The azimuth filter is a nonrecursive convolution-type bandpass filter. The optimum filter bandwidth in terms of resolution and signal-to-noise ratio would be a function of the square root of range. A substantial hardware savings and only a minor loss of performance result from choosing the bandwidth to be independent of range. An aircraft-velocity-dependent bandwidth is not difficult to implement. Such an implementation causes the final display resolution to be independent of aircraft velocity.

Clutter lock.—During normal operating conditions, the antenna will not always be directed normal to the flightpath. High crosswinds will cause the aircraft heading and the flightpath to differ by several degrees. Because of such a drift angle, the azimuth clutter spectrum is no longer centered on zero Doppler (fig. 5-22). Also, the resulting offset frequency f_{offset} is not constant but de-

pends on range. If the clutter spectrum is not centered on zero Doppler, the azimuth filters designed to filter near-zero Doppler may not function correctly. Two basic approaches to the frequency-offset problem are possible. One approach would use aircraft drift angle and altitude and calculate a correction frequency as a function of range. (The drift-angle input from the aircraft would have to be accurate to approximately 0.1° .) The azimuth filters may then be re-centered on the main loads of the return spectrum. A second approach would measure the offset frequency from the clutter return and correct accordingly. The latter approach is generally recommended for these radars. Special effort is necessary to insure that very large point targets do not introduce false offset errors as they enter or leave the antenna pattern.

Motion compensation.—For coherent or synthetic aperture mapping radar systems, it is preferable that the aircraft fly in a perfectly straight line. The target azimuth phase histories would then be predictable and easily processed for improved resolution. Aircraft usually do not follow perfectly straight-line flightpaths. Deviations from the straight-line flightpath produce errors in the phase history of any target echo. These errors may be corrected by using crosstrack and vertical accelerometers on the antenna. The accelerometer outputs may be high-pass-filtered and integrated to measure crosstrack displacements, which, in turn, may be used to calculate range errors. Range errors are converted to phase errors, and the necessary corrections are generated as a function of range.

Recorder.—Real-time wet chemical film processors are now used on some mapping radars. Recent developments in dry-film processing and fiber optics make it feasible to consider the development of a real-time dry-film-processing camera for mapping radar data. This development would reduce operating costs and minimize storing and handling of corrosive monobath chemicals.

Dry silver film, now available commer-

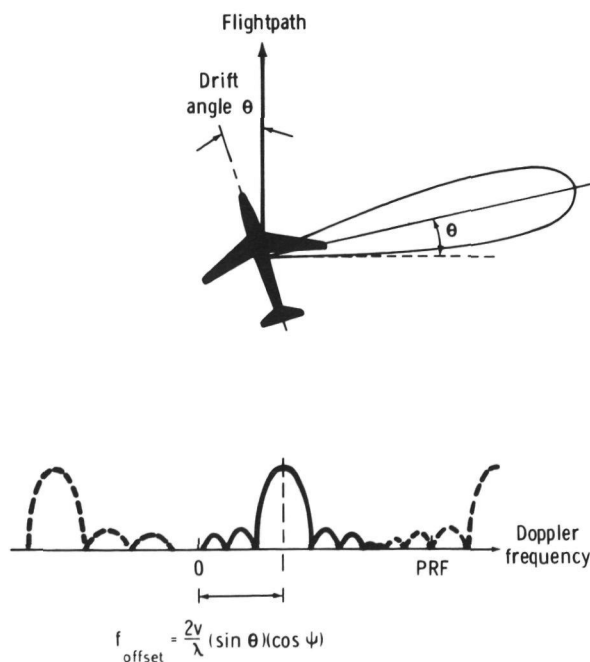


FIGURE 5-22.—Effect of drift angle on antenna direction and azimuth clutter spectrum, where v is aircraft velocity, λ is transmitted wavelength, and ψ is depression angle to target.

cially, uses heat processing rather than the wet monobath developing. However, this dry film has a lower sensitivity than wet-processing film, which means that the radar image recorder must provide higher light levels to properly expose the film. New design concepts include the use of a CRT with high-intensity phosphors and fiber-optic faceplates. The dry silver film is exposed by moving it directly over the fiber optics. The fiber-optics technique provides an increase in the percentage of light gathered from the CRT phosphor and applied to the film. Previously used double-lens optical systems, using an $f/1.4$ lens, direct approximately 5 percent of the available light onto the film. A fiber-optics system could increase this technique to near-70-percent efficiency. Dry silver film is developed and fixed by passing it over a heated plate. The radar image could then be available for near-real-time viewing.

Special Applications of SLAR Image Data

A detailed geologic evaluation of 25-cm (L-band) SLAR images obtained over Death Valley, California, was recently completed (ref. 5-1). This study is a good example of the type necessary to properly quantize and characterize the poorly understood interaction of active microwave signals with a terrain interface having diverse roughness scales. The following is a summary of the work represented in reference 5-1.

Summary of Death Valley Study

The salt flats and large gravel fans that characterize the floor of Death Valley, California, produce sensitive 25-cm radar-backscatter variations (image gray tone) that are correlated with systematic changes in surface-roughness parameters. The large range (0.01 to 2 times the wavelength of 25 cm) in "Lambert" and "Lommel-Seelinger" type surface roughness permitted a detailed investigation of the irregularity scale causing the change from diffuse to specular radar backscatter as theorized by the Rayleigh criterion. The agreement was

good, and the transition point was found to be more clearly identified with a specific size range of surface irregularity than it was previously thought to be.

Backscatter variations within Death Valley very well describe the previously mapped geologic units, and it is suggested that long-wavelength radar systems are scientifically optimized for surface roughness investigation when antenna depression angles are restricted between 45° and 90° .

A major conclusion is that an airborne or spacecraft multifrequency radar system should provide image data of significant land use and economic resource potential, especially over the 680 million acres of extremely arid to semiarid lands in the United States.

Experiment Description

During the spring of 1969 and 1970, 25-cm-wavelength side-looking radar images covering a total of 13 300 km² were obtained over Death Valley. These flights, including both east- and west-look directions, were intended as system function tests of a prototype planetary imaging radar.

The radar system¹ was operated in a side-looking mode with a unique 0° to 45° look angle off vertical and with a slotted antenna array. Horizontally polarized radiation was transmitted, and horizontally polarized backscatter was recorded on 35-mm film, which was processed by optical correlation techniques. The radar equipment was flown aboard a NASA Convair 990 jet aircraft² operated by the Airborne Sciences Office of Ames Research Center in Mountain View, Calif.

The Death Valley area was chosen as the radar system calibration site because of the nearly total lack of leafy vegetation on the Death Valley floor and the extremely low

¹Synthetic aperture optical recorder: 70- μ sec sweep (transmitter 10-MHz sweep in 1.5 μ sec); 6-kW peak power; 15-W average power; 18° antenna beamwidth in azimuth looking forward and 9° looking back; 1215-MHz frequency.

²The 1970 flight, south run: 7925-m altitude; 254-m/sec speed. The 1970 flight, north run: 3048-m altitude; 200-m/sec speed.

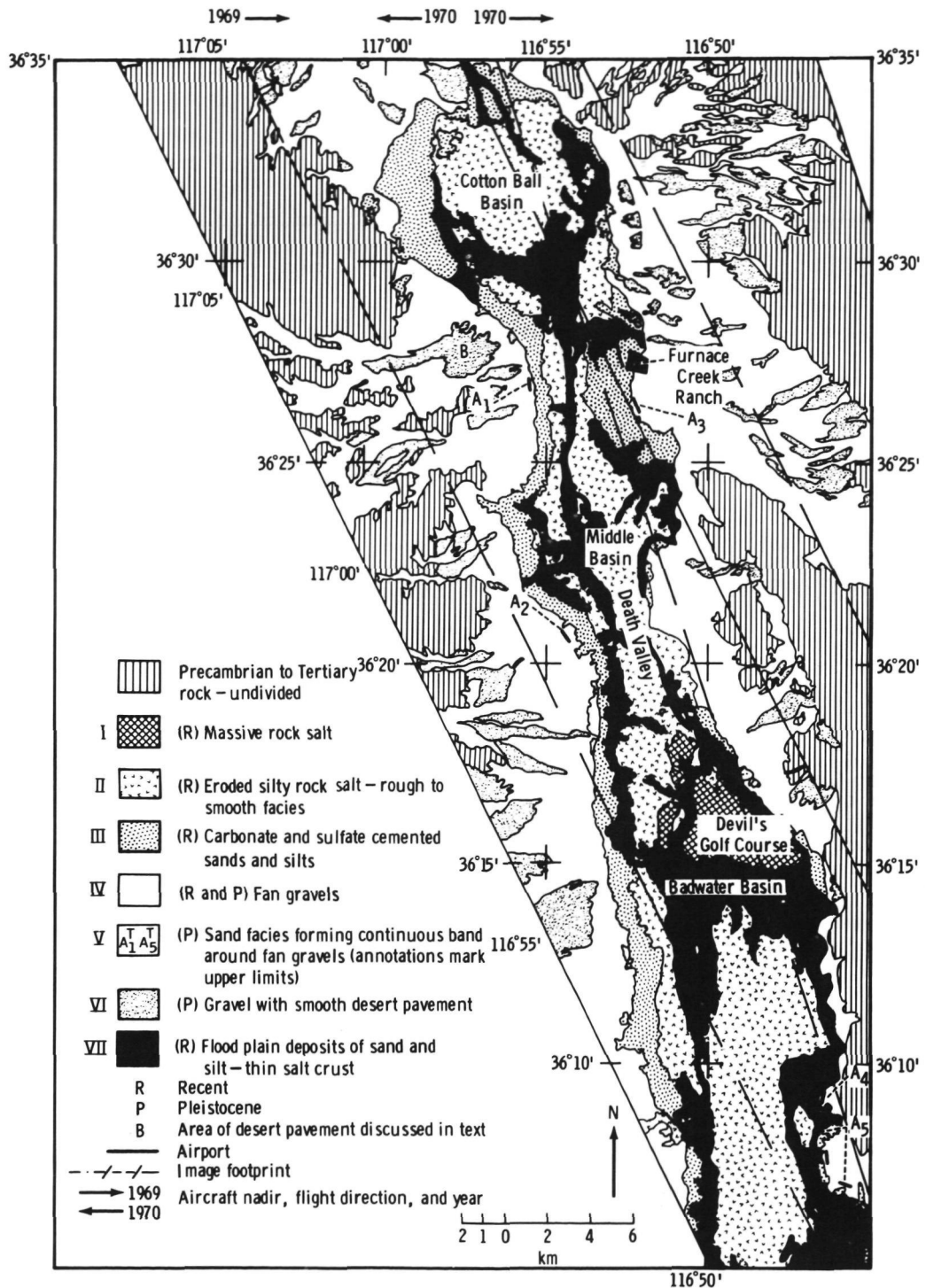


FIGURE 5-23.—Index map of Death Valley showing correlation of geology with 25-cm backscatter units (I, most diffuse; VII, most specular). See figure 5-24.

(4 cm/yr) precipitation rate. Death Valley has also been well described from geological (ref. 5-2), hydrological (ref. 5-3), and botanical (ref. 5-4) viewpoints.

The scale of the original 35-mm radar image film is approximately 1:600 000, although that portion of the crosstrack image nearest the flight line is considerably foreshortened because of inherent characteristics of the image acquisition and processing techniques. Ground resolution in range is approximately 60 to 100 m at the 45° incident angle, whereas azimuth resolution at any angle is approximately 20 m.

Schaber and Brown (ref. 5-5) discussed the geological potential of images obtained near Flagstaff, Ariz., with the same 25-cm-wavelength radar system, and a discussion of the effect of surface textures and complex

dielectric constant on (10° to 70° look angle) K-band (0.86-cm wavelength) SLAR images of arid regions has been published by MacDonald and Waite (ref. 5-6).

The Death Valley investigation includes detailed roughness-calibrated radar response from many distinct sedimentary surfaces on the giant gravel fans and salt pans characterizing the extremely arid Death Valley floor.

Characterization of Geological Units on the Radar Images

Figure 5-23 is a generalized geological map of Death Valley (ref. 5-2) illustrating seven major geological surfaces clearly defined by backscatter variations on the 25-cm radar images shown in figure 5-24.

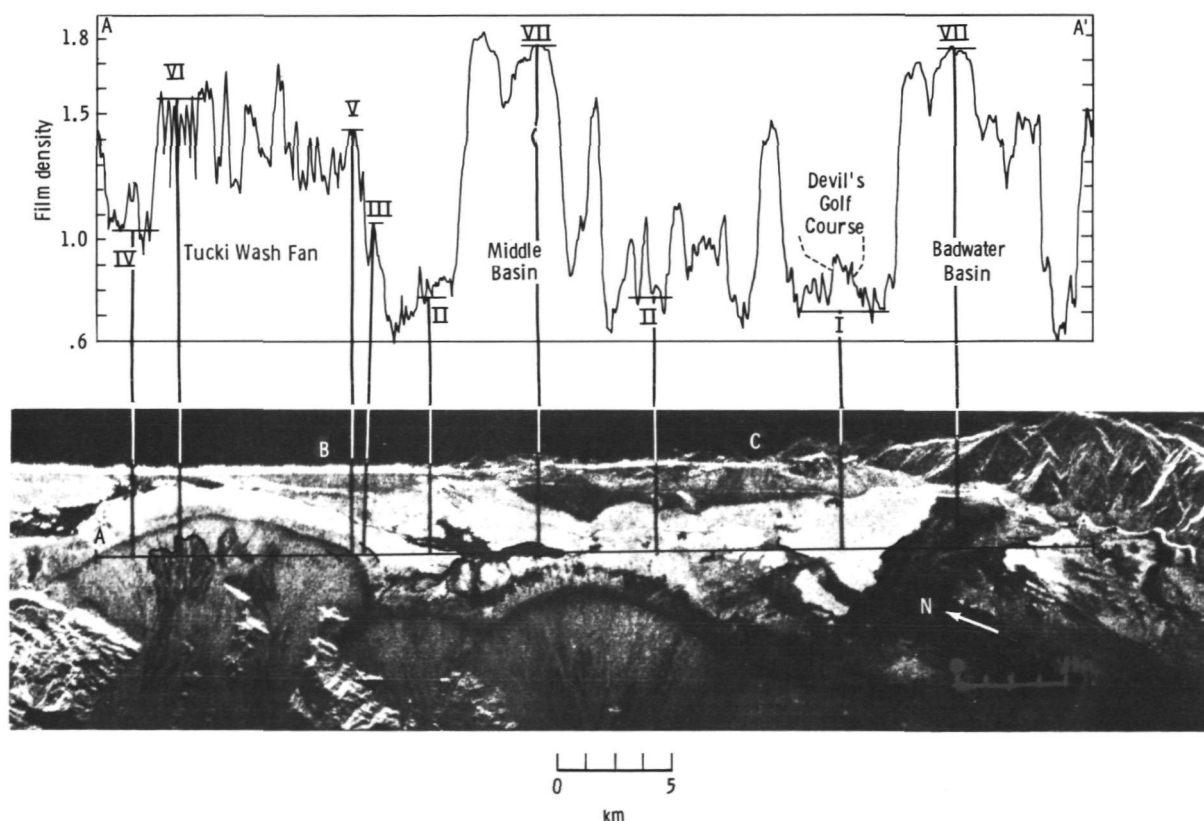


FIGURE 5-24.—West-looking radar image (25 cm) of Death Valley showing correlation of radar backscatter units I to VII with film photometric scan data taken at indicated profile A to A'. The profile is 32.7 km long.

Unit I is the highest backscattering flat-lying surface on the images and covers the least areal extent within Death Valley (20.7 km²). This unit is represented by the Devil's Golf Course at Badwater and is composed of Quaternary massive rock salt with an extremely rough surface that elevated and protected against seasonal flooding. Vegetation of any kind is virtually absent (fig. 5-25(a), 5-25(b), and 5-25(c)).

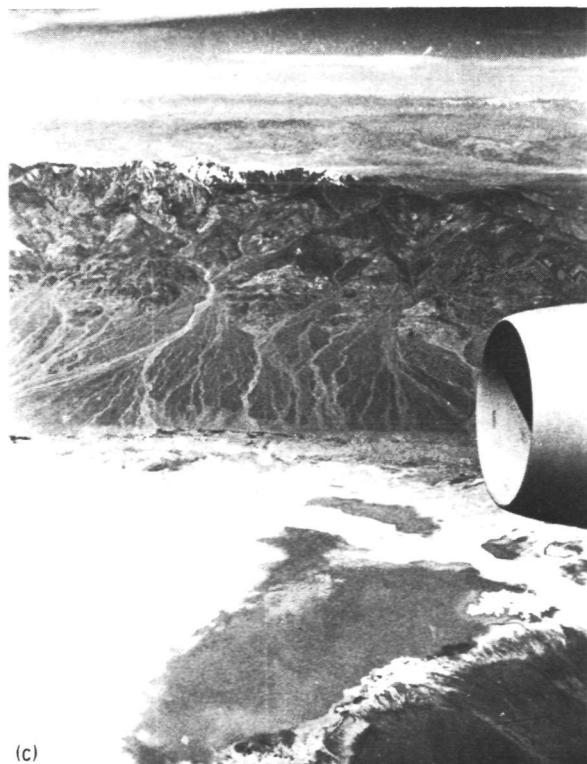
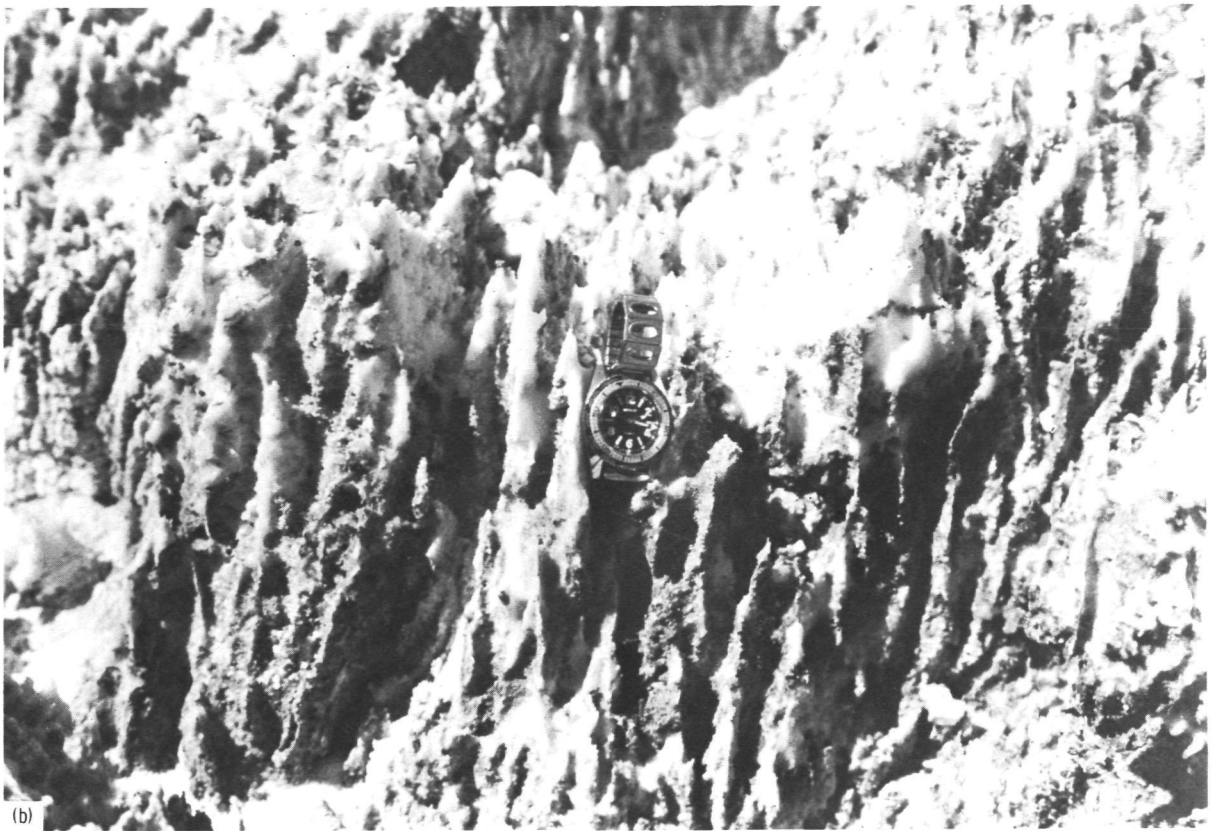
Three additional decreasing rough facies of the Quaternary chloride zone are grouped

together in figure 5-23 as unit II (fig. 5-26(a) and 5-26(b)). All facies listed in unit II are lacking in vegetation.

The third highest backscattering, unit III, delineated on the radar images is composed of two facies of Quaternary carbonate salt-impregnated Pleistocene lake deposits and five facies of miscellaneous Quaternary sulfate and carbonate salts (fig. 5-27(a) and 5-27(b)). Pickleweed and several species of phreatophytes having brine affinities comprise the sparse vegetation.



FIGURE 5-25.—Photographs of Devil's Golf Course (unit I) shown in geological map (fig. 5-23) and radar image (fig. 5-24). (a) Landscape photograph of massive rock salt of the Devil's Golf Course (unit I) that gave a highly diffuse (nearly isotropic) backscatter over incident angles ranging from 12° to 40°. Gnomon has wand length 31 cm above tripod base, gray-tone chart on gnomon leg is divided into 2.5-cm increments; black rule has small divisions of 1 cm and large divisions of 5 cm.



**ORIGINAL PAGE IS
OF POOR QUALITY**

FIGURE 5-25 (concluded).—Photographs of Devil's Golf Course (unit I) shown in geological map (fig. 5-23) and radar image (fig. 5-24). (b) Closeup view of extreme 2- to 3-cm ($\lambda/10$) roughness. (c) Aerial view of Devil's Golf Course (dark heart-shaped unit) taken during radar overflight. Notice the reversal photographic and radar albedos for Devil's Golf Course (unit I) and flood plain (unit VII) (fig. 5-24).



FIGURE 5-26.—Photographs of silty rock salt with rough facies (20 to 40 percent silt) that gave highest backscatter within unit II (fig. 5-24). Gnomon has wand length 31 cm above tripod base; gray-tone chart on gnomon leg is divided into 2.5-cm increments; black rule has small divisions of 1 cm and large divisions of 5 cm.
(a) Landscape photograph.

Unit IV is limited to only the younger of the Upper Pleistocene and Recent gravels of the giant gravel fans. The Pleistocene materials are loose pebble-to-cobble-size varnished gravel with significant concentrations of boulders (fig. 5-28). Although not varnished, the Recent fan gravels are similar and exist in washes as much as 3 m below the level of the older Pleistocene materials.

Unit V represents the only distinct radar signature on the images that could not be related to a specifically mapped geological material. This unit is imaged as a narrow (100 to 200 m wide) dark band that is consistently found at the very base of the gravel fans in contact with the high backscattering unit III of the Death Valley salt pan (fig. 5-24). An-

other characteristic of the dark band on the images is that it is generally darkest (greater film density and weakest backscatter) at the very base of the gravel fans and becomes more diffuse (reduced film density and increased backscatter) within a few hundred meters toward the head of the fan. Field investigation revealed that the dark band was resulting from weak signal return from a boulder-free sandy zone distinguished by a lag of small rock fragments (fig. 5-29) that becomes systematically larger upslope on the fan. The relationship of gravel size to backscatter power within unit V will be discussed later in this section.

The relatively low backscattering (unit VI) was unexpectedly found to be well cor-

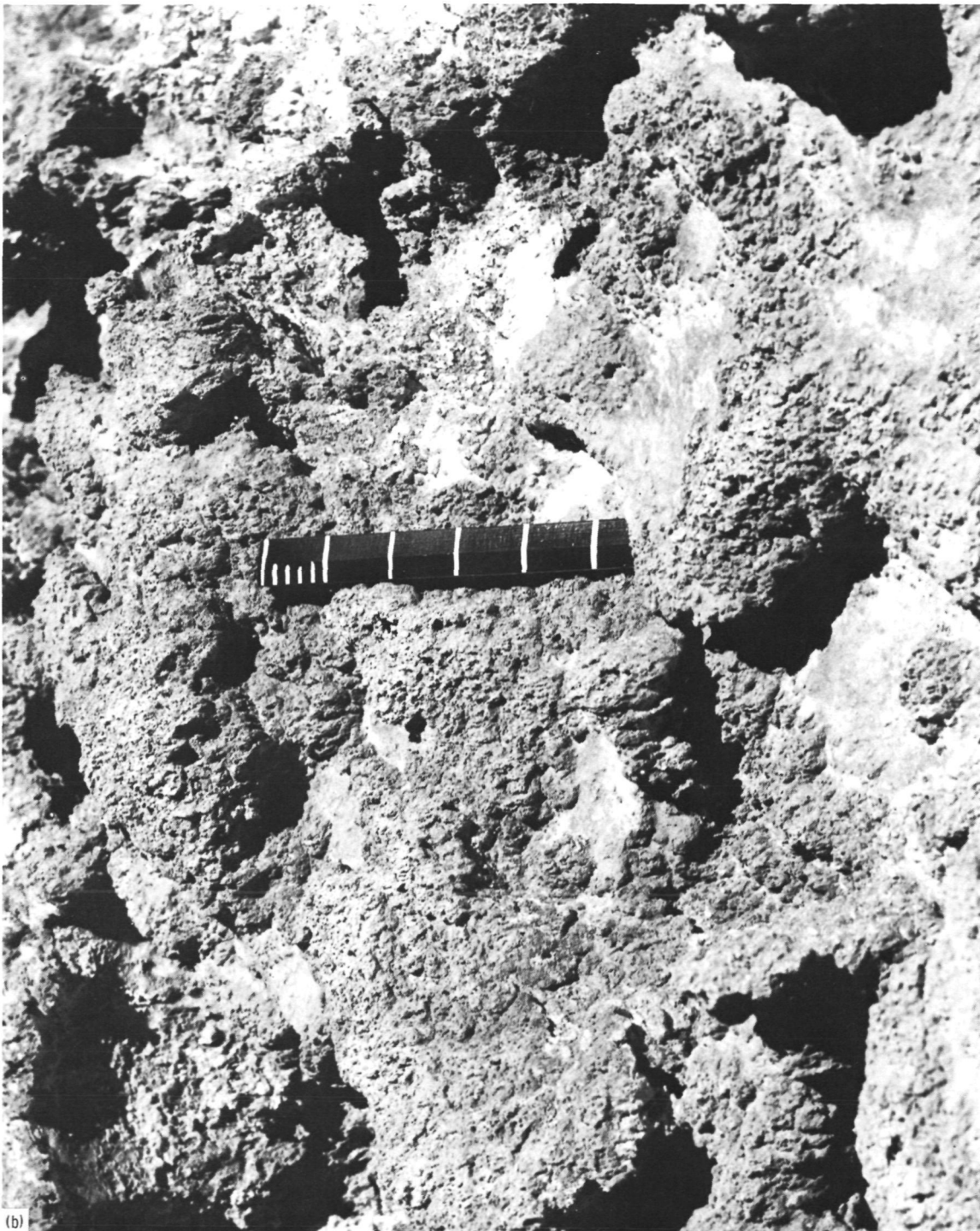


FIGURE 5-26 (concluded).—Photographs of silty rock salt with rough facies (20 to 40 percent silt) that gave highest backscatter within unit II (fig. 5-24). Gnomon has wand length 31 cm above tripod base; gray-tone chart on gnomon leg is divided into 2.5-cm increments; black rule has small divisions of 1 cm and large divisions of 5 cm. (b) Closeup view; small-scale roughness at 1 to 2 cm equal dimensional hummocks of silt.

ORIGINAL PAGE IS
OF POOR QUALITY

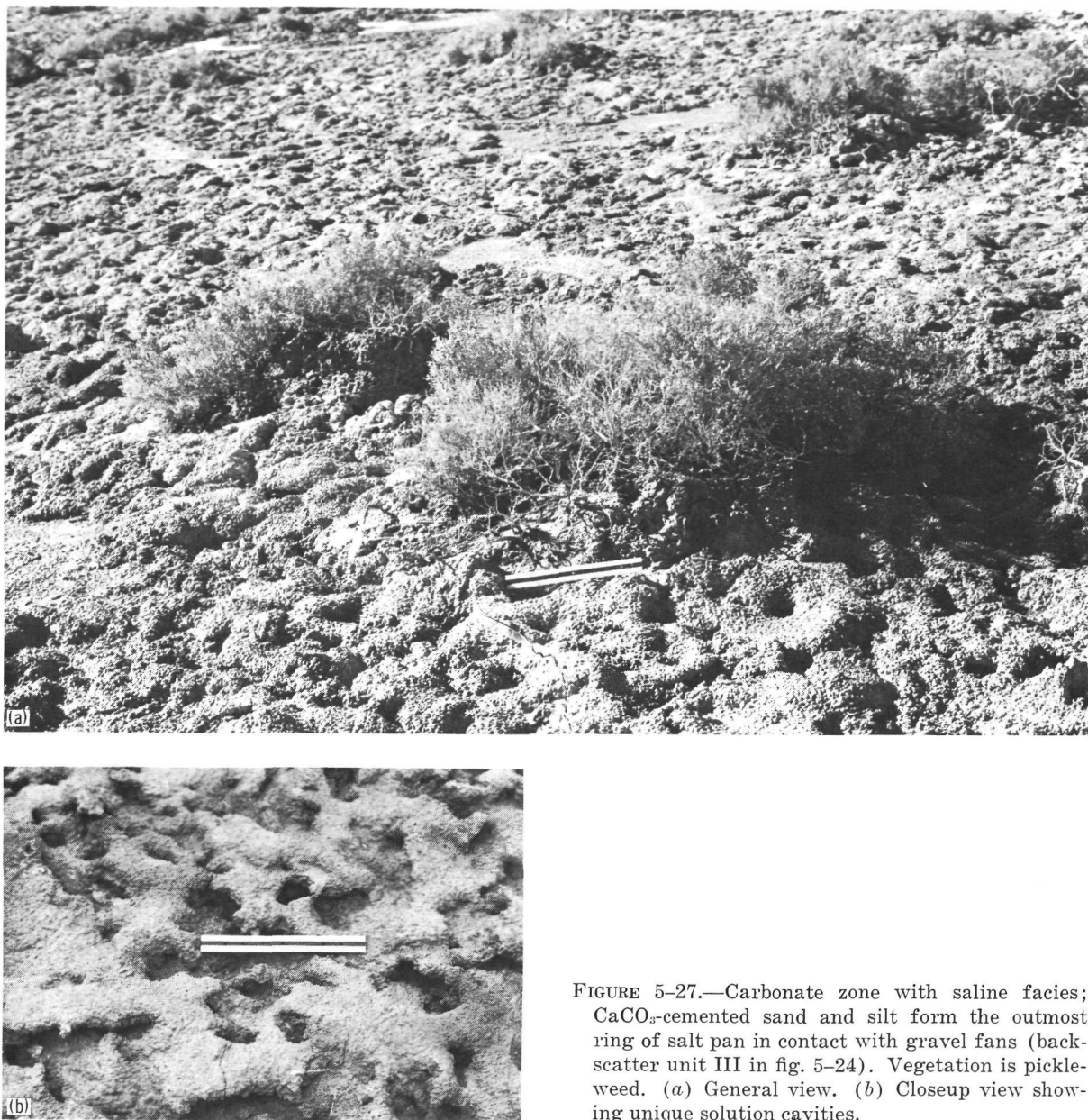


FIGURE 5-27.—Carbonate zone with saline facies; CaCO_3 -cemented sand and silt form the outmost ring of salt pan in contact with gravel fans (backscatter unit III in fig. 5-24). Vegetation is pickleweed. (a) General view. (b) Closeup view showing unique solution cavities.

related with the oldest of the Upper Pleistocene fan gravels (figs. 5-23 and 5-24). The reason for such anomalous radar behavior lies in the fact that the unit VI surface is smooth "desert pavement," whereas the younger gravels have rough surfaces. The boulders and cobbles forming the original surface of these deposits have disintegrated to produce smaller, angular rock fragments.

The "fitting together" of these weathering products forms the smoothest desert pavements in Death Valley (fig. 5-30). The desert-pavement surfaces are elevated above the present Recent washes near the head of the fans. Excellent representation of the desert pavement (unit VI) on radar images as compared to conventional photography is shown in figures 5-31 and 5-32(a), 5-32(b),



FIGURE 5-28.—Younger of the upper Pleistocene boulder gravels forming giant alluvial fans (radar unit IV). Notebook (21 cm long) is shown in foreground.

and 5-32(c). Vegetation is lacking except for xerophytes along the washes.

The lowest backscattering material in Death Valley is referred to as unit VII and is represented by the Recent flood-plain deposits that seasonally flood the lower parts of the Death Valley salt pan (figs. 5-23, 5-24, and 5-33). The floodplains are mostly flat and level expanses of occasionally damp or brine-soaked sandy silt and clay; part is encrusted with salt. The salt crust on the floodplain ranges from a thin delicate efflorescence to a firm crust several centimeters thick (ref. 5-2).

Surface Roughness Data and Correlation With Radar Backscatter

Theories pertaining to scattering of microwave signals from terrain have been the subject of much discussion for many years (refs.

5-6 to 5-10). The only two terrain parameters affecting the radar-scattering coefficient are surface roughness and the complex permittivity. Almost all workers agree that surface roughness is the dominant causative factor in amplitude variation of the returned signal (effecting image gray tone). Radiated energy is reflected in a specular (mirror-like) manner, according to Snell's Law, from a "smooth" surface and is reflected in a diffuse (energy scattered in all directions) manner from a "rough" surface. The question usually encountered in interpretation of SLAR images concerns the scale of roughness necessary to change from specular (smooth) to diffuse (rough) scattering. One of the major objectives of the Death Valley radar study was to approach this question from an empirical rather than a theoretical viewpoint.



FIGURE 5-29.—Closeup view of small-scale surface lag and underlying loose sand characteristic of the base of radar unit V. This surface was dominated by specular reflectivity.

The most quoted theoretical relationship with regard to radar “smoothness” is the so-called Rayleigh criterion that considers a surface “smooth” for

$$h < \frac{\lambda}{8 \sin \gamma} \quad (5-12)$$

where h is height of surface irregularities, λ is wavelength of radar system, and γ is grazing angle of the incident radar wave.

In deriving this criterion, Rayleigh considered rays 1 and 2 (fig. 5-34) incident on a surface with irregularities of height h at a grazing angle γ . The path difference between the two rays is expressed as

$$\Delta r = 2h \sin \gamma \quad (5-13)$$

and the phase difference is expressed as

$$\Delta \phi = \frac{2\pi}{\lambda} \Delta r = \frac{4\pi h \sin \gamma}{\lambda} \quad (5-14)$$

Rayleigh thus argued that for $\Delta \phi = \pi$, the surface is “rough,” whereas, for $\Delta \phi = 0$, it reflects specularly and is “smooth.” In obtaining the Rayleigh criterion, an arbitrary choice halfway between the two examples (i.e., $\Delta \phi = \pi/2$) is made to represent the transition from diffuse to specular backscatter.

Peake and Oliver (ref. 5-7) used a truck-mounted radar-radiometer system to compare radar backscatter variation with change in a normalized roughness parameter ξ for three frequencies (X-, Ku-, and Ka-bands), where

$$\xi = \frac{d \cos \theta_i}{\lambda} \quad (5-15)$$

and where d is particle diameter, θ_i is angle



FIGURE 5-30.—Desert pavement (“varnished”) formed on surface of oldest of upper Pleistocene fan gravels (radar unit VI). Surface of pavement rocks extremely polished.

of incidence, and λ is wavelength. These researchers found that the transition between specular and diffuse scattering occurs at approximately $\xi=0.3$. This value appears to be slightly large for the 25-cm SLAR data of Death Valley.

Absolute calibration of the radar return power was not obtained during the Death Valley overflights. Therefore, relative exposure energies were obtained from the film (type 3414) $D \log_e$ sensitometry curve (fig. 5-35).

To quantitatively evaluate the relationship between relative return power and surface-roughness parameters, a total of 11 photometric scans were made across various regions of the radar images. Figure 5-24 illustrates the clear variations in film density

observed for the seven major radar-backscatter units described previously. Table 5-VIII lists the physical roughness parameters for these seven radar terrain units and the relative power (dB) values representative of each. In figure 5-36, these data are plotted with relative radar power as a function of the sum of parameters A , B , and C (at $\lambda/10$ scale) for each of the seven radar terrain units. Average vertical roughness ranges from approximately 0.01 to 2λ .

The significant aspects of figure 5-36 are the two distinct curve slopes with the inflection occurring at a vertical roughness representative of approximately 3 to 5 cm. It appears from this correlation that the change-over from primarily diffuse (rough) to pri-

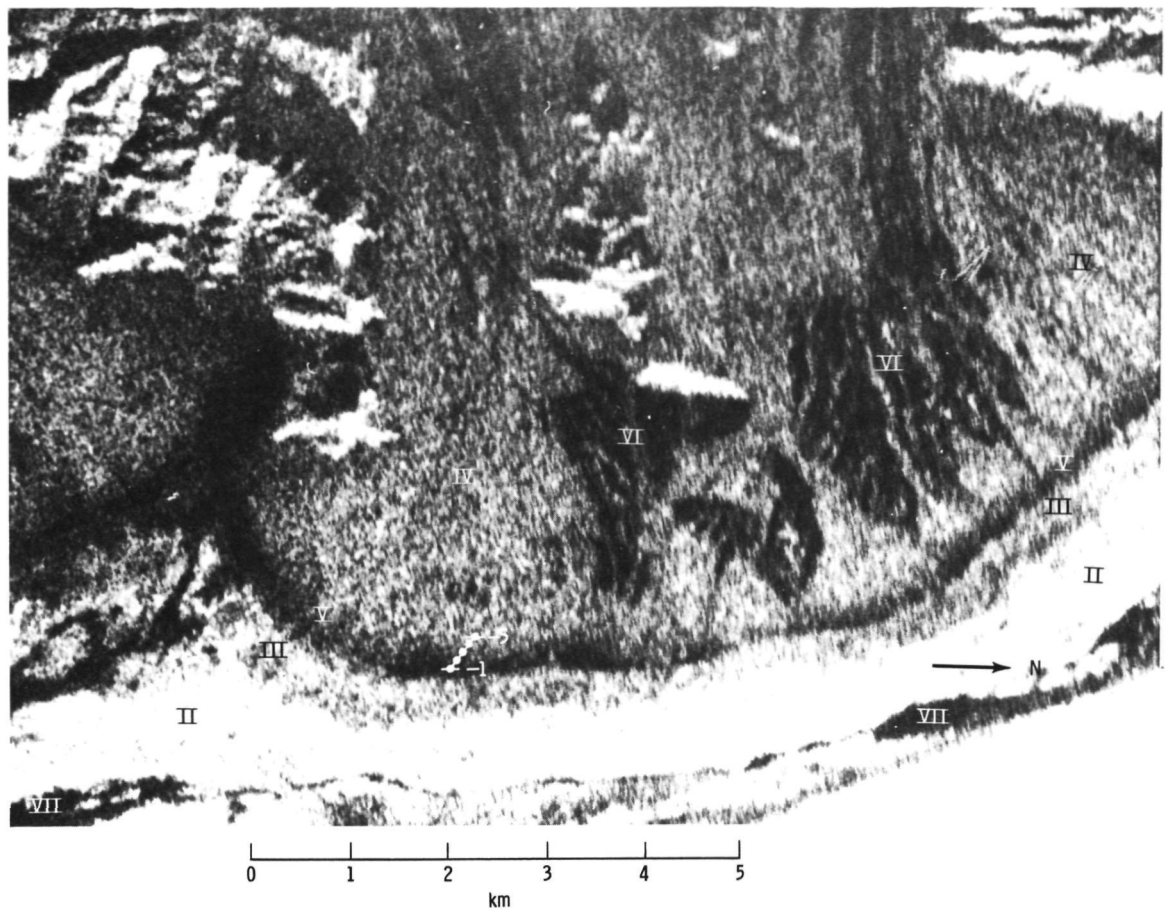


FIGURE 5-31.—Enlargement of west-looking 25-cm radar image of Tucki Wash gravel fan. Roman numerals represent radar backscatter units. Dots indicate sample locations 1 to 5.

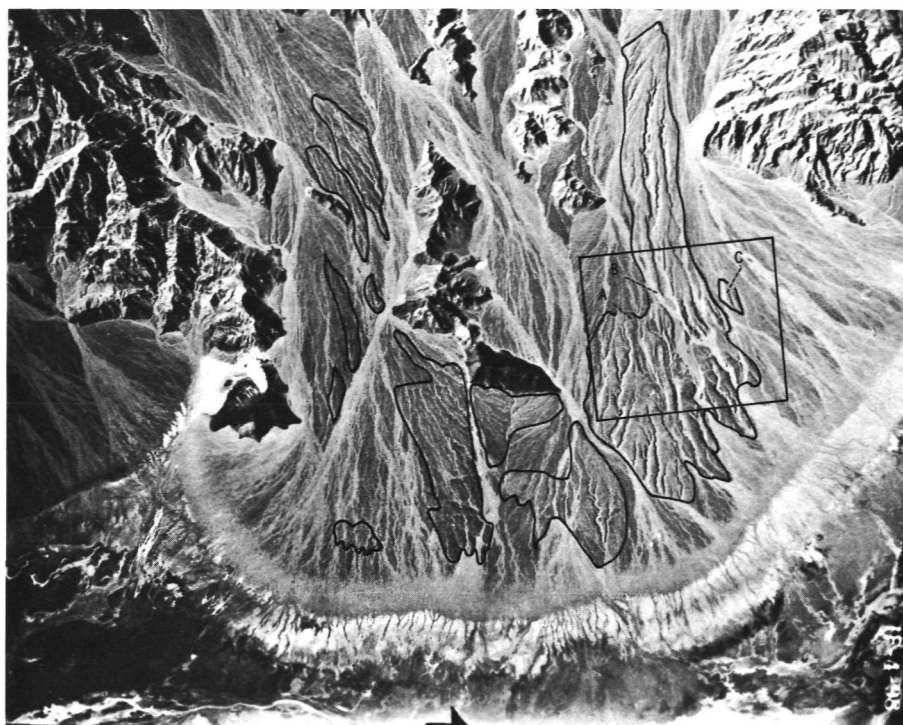
TABLE 5-VIII.—*Roughness Parameters and Relative Backscatter Power*

Backscatter unit	Parameter A: macrovertical relief, cm ^a	Parameter B: average distance between macrorelief facets, cm ^a	Parameter C: percent area covered by microroughness ^{a b}	Roughness parameter α ^c	Film density	Relative power, dB
I	49.0	60.0	100.0	209.0	0.700	0.0
II	29.0	44.0	97.0	170.0	.749	-.4
III	6.0	15.0	20.0	42.0	1.163	-2.4
IV	12.0	10.0	40.0	62.0	1.266	-3.0
V	1.5	6.0	15.0	22.5	1.580	-4.4
VI	1.0	2.0	8.0	11.0	1.600	-4.5
VII2	2.0	.0	2.2	1.756	-5.3

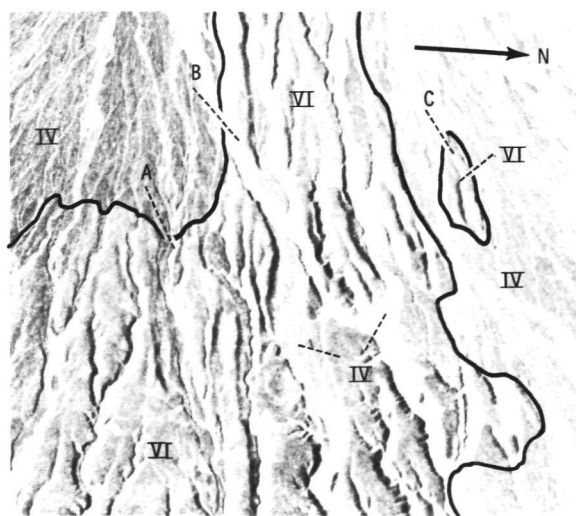
^a Roughness parameters A, B, and C represent averages of many field measurements.

^b at $\lambda/10$ scale.

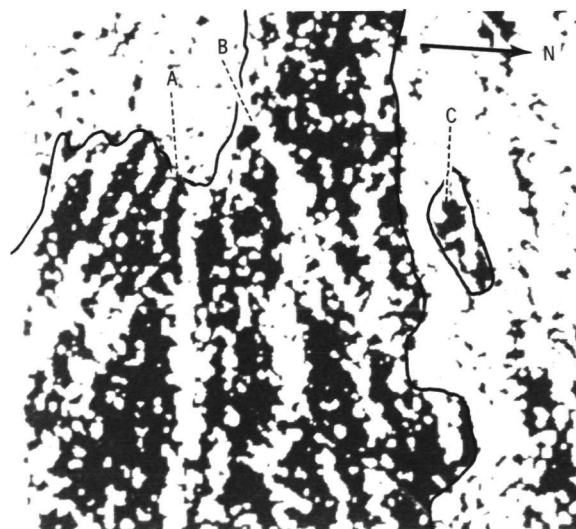
^c Parameter α equals the sum of parameters A, B, and C.



(a)



(b)



(c)

FIGURE 5-32.—Photographs of Tucki Wash gravel fan together with computer representation of digitized radar image for designated area. (a) Aerial photograph of Tucki Wash gravel fan with desert pavement regions delineated. Area in rectangle is for reference to figures 5-32(b) and 5-32(c). Points A, B, and C designate recent washes. (b) Enlargement of area indicated in figure 5-32(a). Recent washes are indicated at points A and B and outer part of desert pavement at point C. (c) Computer representation of digitized radar image of same area shown in figure 5-32(b) (processed to enhance pavement region). Note points A, B, and C. Computer enhancement performed at Jet Propulsion Laboratory Image Processing Laboratory.

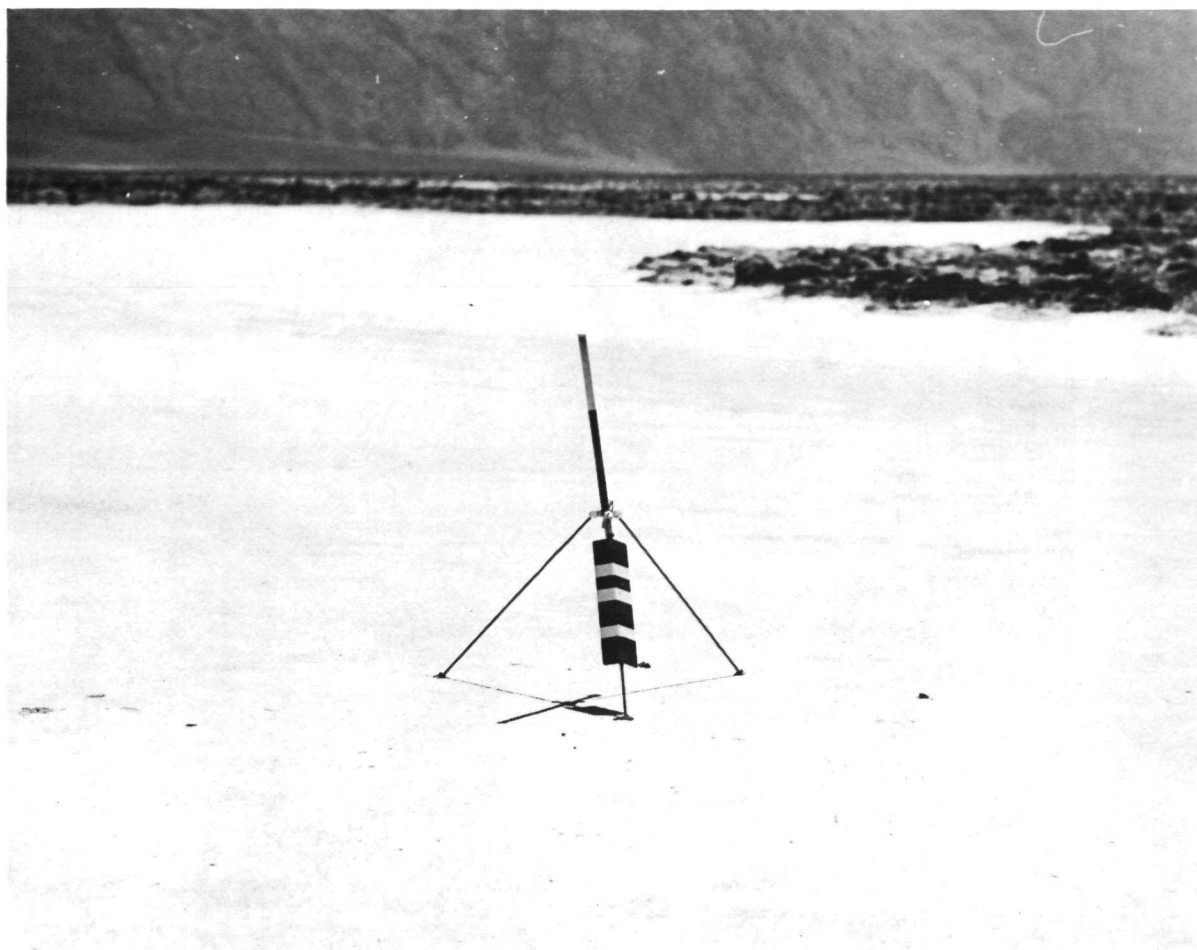


FIGURE 5-33.—Recent flood-plain surface (radar unit VII) giving essentially no radar return. Surface is coated with less than 1 cm of sodium chloride. Surface in background is eroded rock salt that is 15 cm higher than flood plain.

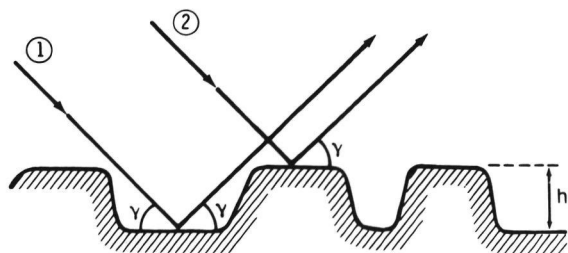


FIGURE 5-34.—Derivation of the Rayleigh criterion (after Beckmann and Spizzichino (ref. 5-10)). Numbers 1 and 2 represent incident rays.

marily specular (smooth) scattering may occur rather abruptly.

Two distinct types of surface roughnesses within Death Valley have made this region ideal for a detailed investigation of radar-scattering processes. The first is the chemical or solution roughness of the salt facies characterizing the salt pan of Death Valley floor (units I, II, and III) (figs. 5-25, 5-26, and 5-27). These surfaces have extremely rough reentrant cavities, with the concordant high points forming a flat and level plain on the scale of several meters. These salt-pan surfaces appear to be perfect examples of a "Lambert" roughness.

The second form of roughness encountered within Death Valley is that characteristic of

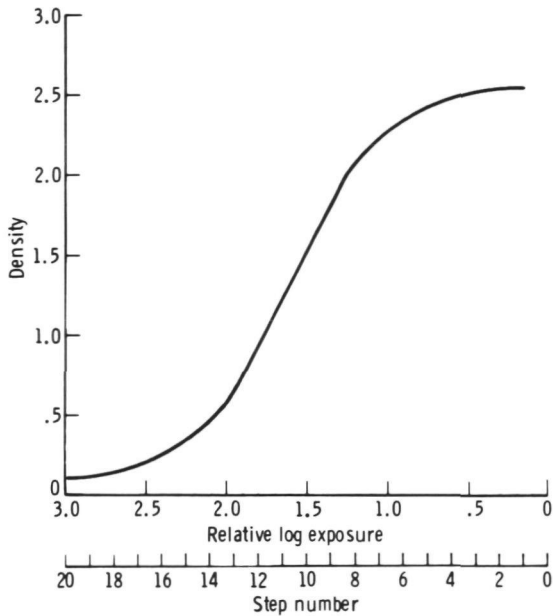


FIGURE 5-35.—Sensitometry curve $D \log_e$ for the film type and processing used for Death Valley radar images. (Film type: Kodak High Definition Aerial 3414.) Steps equal 1.5-dB increments; 1.0 to 2.0 relative log exposure equals 10 dB.

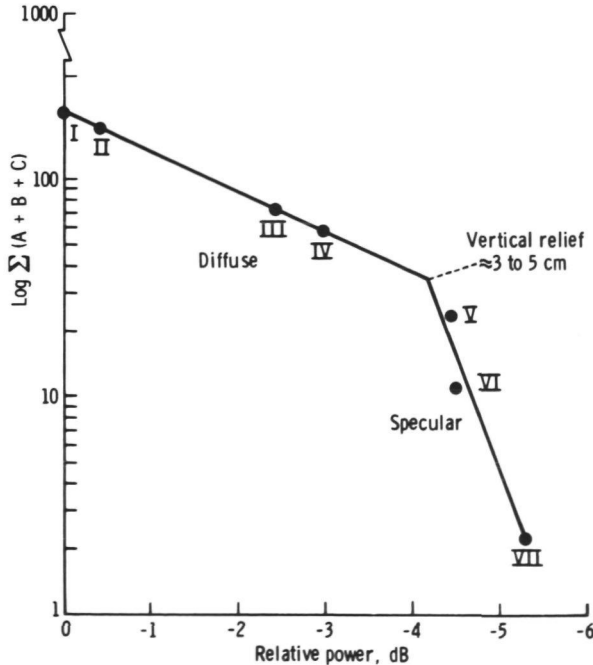


FIGURE 5-36.—Relative power as a function of surface roughness parameters $\log \Sigma(A+B+C)$ for each of the seven radar terrain units.

the giant gravel fans. The gently sloping (2.5°) fans have a generally flat sand and gravel surface on top of which is resting many point scatterers in the form of perched or partly buried cobbles and boulders (fig. 5-28). This type of roughness with many independent point scatterers is called the "Lommel-Seelinger" type (ref. 5-7).

The gravel fans provided a suitable surface on which to quantitatively assess the relationship between frequency distribution of scatterers (rocks) and relative radar power. The gravels were found to be graded by size in a band several hundred meters wide at the base of the fans. The lower portion of this band has earlier been described as the weak radar-backscattering radar unit V (figs. 5-23, 5-24, and 5-31).

Five surface gravel samples (TWF-1 to TWF-5) were collected from 1-m^2 areas, starting at the very base of unit V on the Tucki Wash Fan and extending through this unit up the fan into the larger boulder unit IV for a total distance of 400 m (fig. 5-31). Samples were collected at 100-m intervals together with surface relief data. Figure 5-37 illustrates the presampling distribution of the gravels within each 1-m^2 sample station. Figure 5-38 shows the cumulative percent of total rocks as a function of mean rock diameters. The rock diameters increase consistently from sample TWF-1 to TWF-5.

The sample site locations annotated on the radar image of the Tucki Wash Fan (fig. 5-31) suggest that the area between samples TWF-2 and TWF-3 is the approximate visual contact between the dark band (unit V) and the lighter, coarser gravel deposits (unit IV). This contact should then represent the transition zone between specular and diffuse scattering. A photometric scan was made along the sampling line, and these data were converted to relative power by means of the film sensitometry curve (fig. 5-35). These data were correlated with both surface relief and rock-size percentages for the sample areas on the Tucki Wash Fan as shown in figures 5-39 and 5-40. Both diagrams indicate that the break in slope characterizing

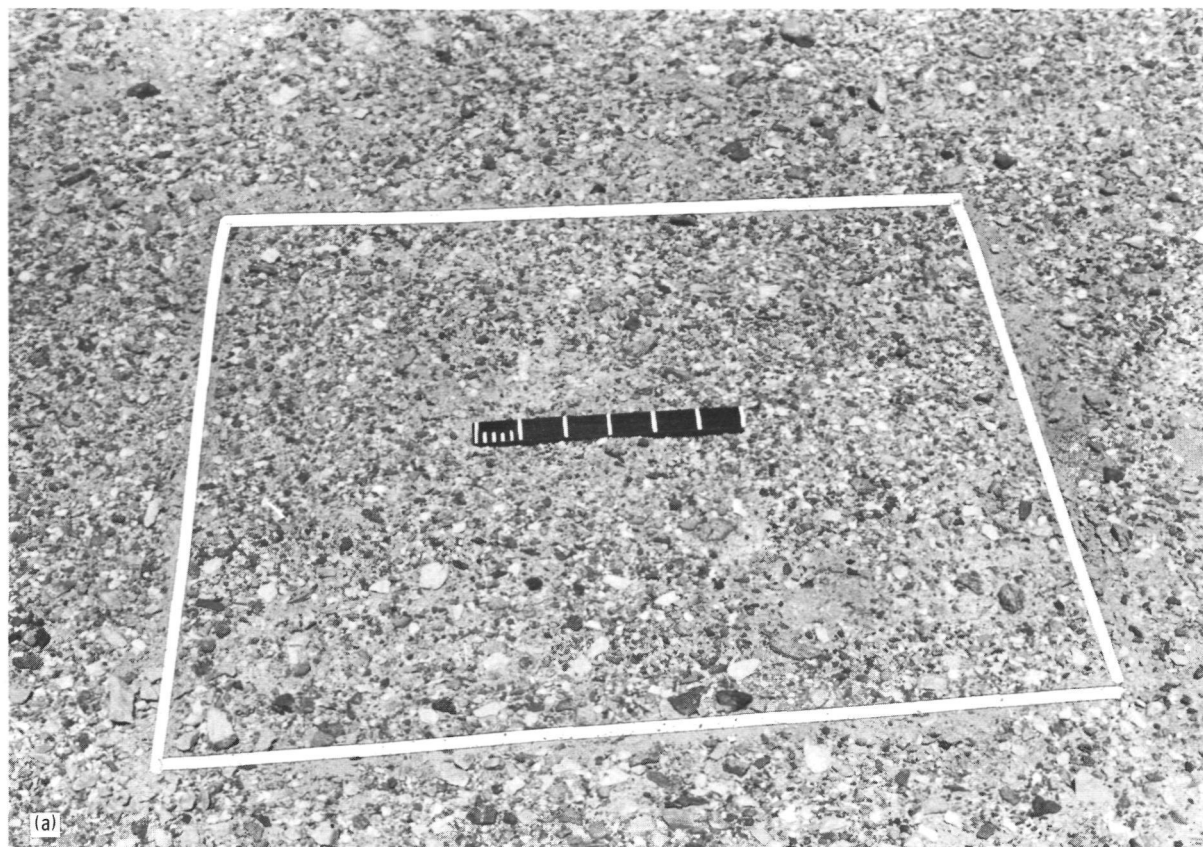


FIGURE 5-37.—Presampling photographs of five 1-m² sample sites (TWF-1 to TWF-5) at the base of Tucki Wash Fan (see fig. 5-31). Samples included all surface lag in 1-m² areas shown by white lines. (a) Sample site 1.

the specular-diffuse transition occurs as visually observed in the region between samples TWF-2 and TWF-3 at approximately the -1.0-dB (relative) power level.

The breaks in slope on figure 5-39 further indicate that 4.1 cm and 6.7 cm should be the minimum and maximum height to characterize the minimum and maximum surface roughness for the initiation of primarily diffuse scattering at 25 cm and at this particular radar grazing angle of 55.62°. The average relief value (4.1 cm) is the same as that shown by the curve inflection in figure 5-36 and is thought to be more significant regarding the radar behavior than the maximum relief data.

To compare this “smooth”/“rough” surface boundary with that of Rayleigh for the

dividing line between “smooth” and “rough” surfaces, the value for the radar grazing angle (55.62°) and the wavelength (25 cm) need only be substituted as

$$h < \frac{25 \text{ cm}}{8 \sin 55.62} \quad (5-16)$$

$$h < 3.8 \text{ cm} \quad (5-17)$$

The value calculated from field measurements of average vertical relief (fig. 5-39) and the theoretical value agree well.

Figures 5-38 and 5-40 show that the cumulative percent of rocks characterizing the transition-zone gravels on Tucki Wash Fan should be as follows: 0.1 percent, $\lambda/2$ (12.5 cm); 5.5 percent, $\lambda/4$ (6.24 cm); 27 percent, $\lambda/8$ (3.125 cm); and 70 percent, $\lambda/16$ (1.562 cm). The mean (50 percent) gravel size



FIGURE 5-37 (continued).—Presampling photographs of five 1-m² sample sites (TWF-1 to TWF-5) at the base of Tucki Wash Fan (see fig. 5-31). Samples included all surface lag in 1-m² areas shown by white lines. (b) Sample site 2.

would be $\lambda/13$, or 1.92 cm. The gravel composing the average surface relief (≈ 4 cm) of the transition zone is equivalent to the larger 25 percent of the bulk gravel sizes.

Peake and Oliver (ref. 5-7) give a normalized roughness parameter of $\xi=0.3$ (eq. (5-15)) for the transition point between specular and diffuse backscatter at the X, Ku, and Ka radar frequencies. The ξ value (fig. 5-39) associated with the average relief transition point is 0.13, or approximately 2.3 times less than that measured by Peake and Oliver. A value of $\xi=0.3$ would give an average surface relief of 9.1 cm by using the normalized roughness relationship of equa-

tion (5-15) (for an incident angle of 34.38° and a wavelength of 25 cm). A surface with this relief in the Death Valley study area is primarily a diffuse scatterer on the 25-cm image data.

Complex Dielectric Constants and Radar Penetration

The rather elevated dielectric constants ϵ of sodium and calcium salts found in the Death Valley salt pan are shown in table 5-IX. Unit III, composed of calcite (CaCO_3) cemented sands and silts, has a surface roughness distinctly less imposing than that

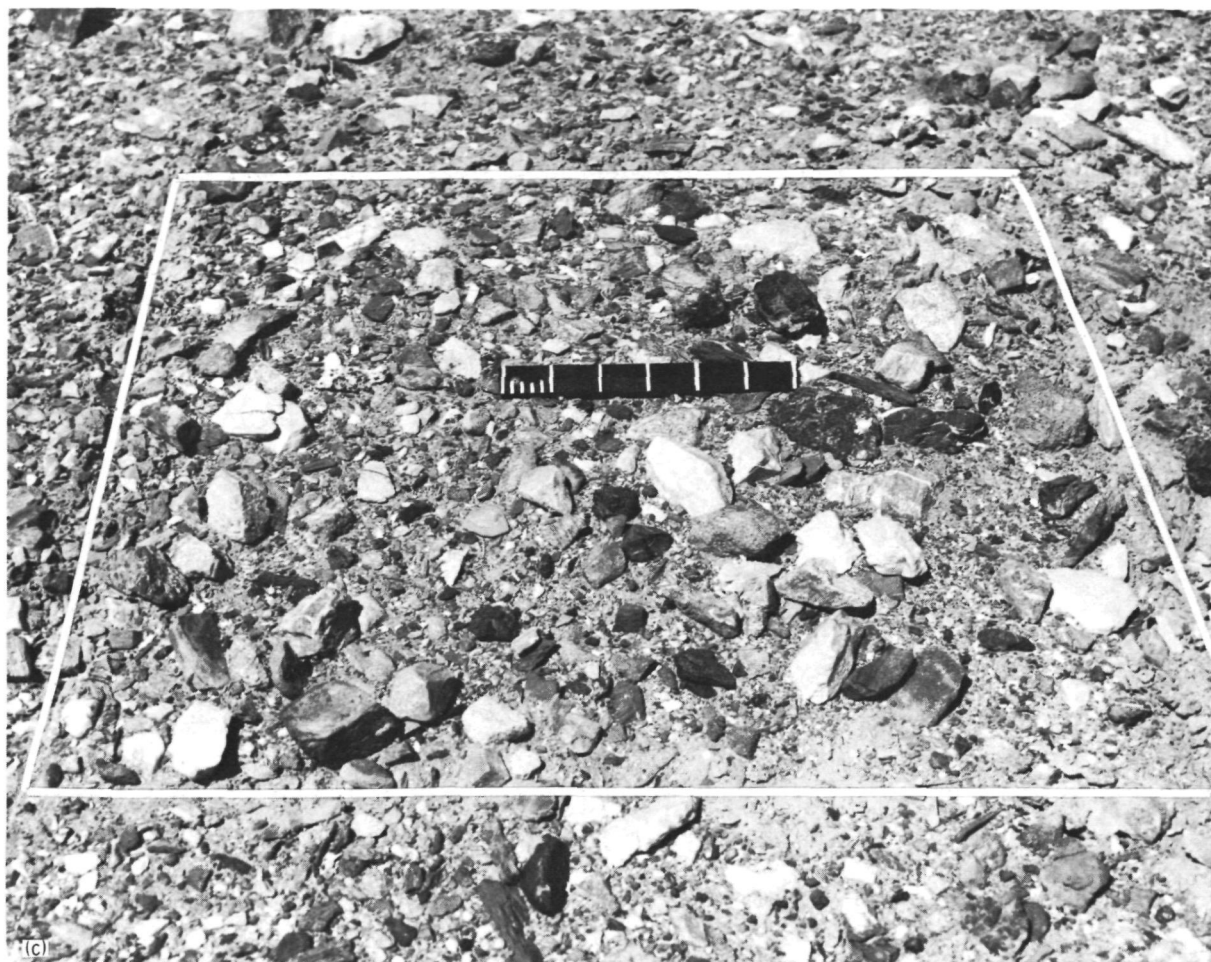


FIGURE 5-37 (continued).—Presampling photographs of five 1-m² sample sites (TWF-1 to TWF-5) at the base of Tucki Wash Fan (see fig. 5-31). Samples included all surface lag in 1-m² areas shown by white lines. (c) Sample site 3.

of the bouldery fan gravels of unit IV (figs. 5-27 and 5-28); however, the backscattering ability in the 25-cm images places the surface roughness slightly above that of the boulder gravel deposits (unit IV) (table 5-VIII). Although these studies have shown clearly that the surface roughness is the dominant cause of the diverse backscatter within Death Valley, there is some evidence to suspect that the elevated ϵ of CaCO_3 and the presence within this material of abundant solution cavities (which cause resonance effects) may be contributing to the abnormally high diffuse return (fig. 5-27(b)). The 25-cm radar may be penetrating a minimum of 0.5 to

1.0 λ (12.5 to 25 cm) into the surface of unit III.

Surface profile data.—The 25-cm radar images also contain high-resolution surface profiles as a result of the 0° to 45° off-nadir angle (fig. 5-24). The vertical range accuracy over flat regions is between 1 and 2 m, but it is somewhat degraded (10 to 20 m) over mountainous terrain because of complexities in the timing reference of signals returning from areas of high vertical relief.

The profiles from smooth, flat surfaces are characterized by “spiking” or fluctuations in the spectral power caused by multiple side lobes (fig. 5-24, point B); this spiking is not



FIGURE 5-37 (continued).—Presampling photographs of five 1-m² sample sites (TWF-1 to TWF-5) at the base of Tucki Wash Fan (see fig. 5-31). Samples included all surface lag in 1-m² areas shown by white lines. (d) Sample site 4.

observed over the rougher mountainous terrains (fig. 5-24, point A). The scientific value of such profiles would be extremely high over regions of little or no photogrammetric control.

TABLE 5-IX.—*Materials Present in Death Valley Salt Pan*

Material	Composition	ϵ (1.0 MHz)
Calcite	CaCO_3	7.5
Halite	NaCl	5.9
Gypsum	$\text{CaSO}_4 \cdot 2\text{H}_2\text{O}$	5 to 11.5
Dry, sandy soil	2.5

Concluding Remarks

The Death Valley region is an excellent area for radar feasibility studies involving detailed geologic analysis of SLAR images. The region is characterized by a variety of materials with diverse dielectric properties and a large range in surface roughness. In addition, the extreme aridity in Death Valley minimizes the effects of vegetation and high soil moisture.

The major conclusions of the present investigation can be summarized as follows:

1. Many types of recent sedimentary surfaces and active sedimentation processes can

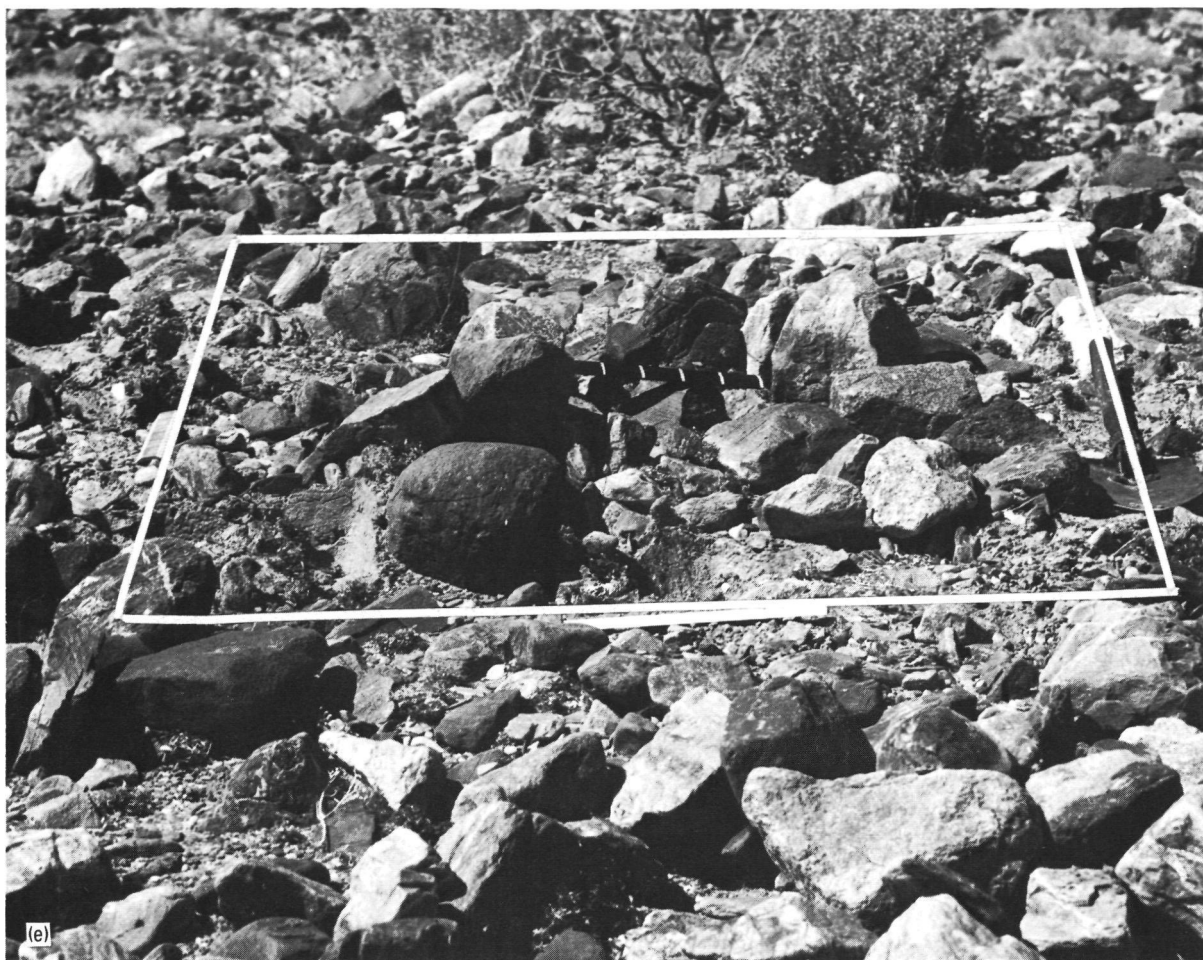


FIGURE 5-37 (concluded).—Presampling photographs of five 1-m² sample sites (TWF-1 to TWF-5) at the base of Tucki Wash Fan (see fig. 5-31). Samples included all surface lag in 1-m² areas shown by white lines. (e) Sample site 5.

be recognized by their surface roughness using only single-frequency SLAR image data. When SLAR is used in conjunction with more conventional sensors, the recognition potential becomes very good.

2. The height of surface irregularities responsible for the transition from specular to diffuse 25-cm radar scattering is restricted to a relatively smaller size range ($\lambda/5$ to $\lambda/8$) than previously thought and is well defined by the assumptions given in the Rayleigh criterion.

3. Antenna depression angles restricted between 45° and 90° appear to optimize the image data for surface backscatter informa-

tion and appear to eliminate extensive radar shadowing effects that distract from geologic material characterization on more conventional SLAR data formats (10° to 70° off-nadir angles).

Future Applications

The radar images evaluated in this section are unique because they were obtained with a prototype of a planetary orbiting radar specifically designed to return high-resolution surface images from the cloud-covered planet Venus, possible in the early 1980's. The investigation of images from the 25-cm system

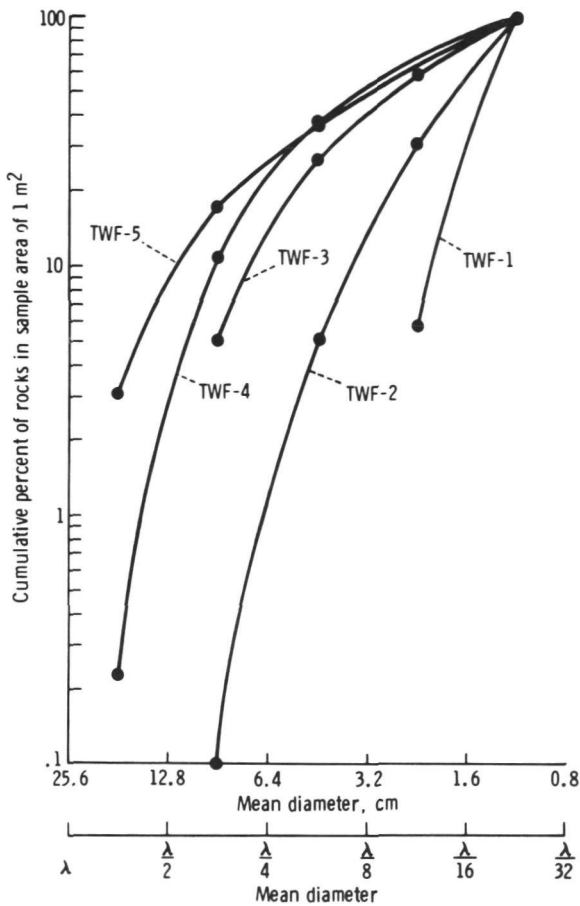


FIGURE 5-38.—Mean diameter of rocks from sample sites TWF-1 to TWF-5 with diameters given in centimeters and λ -ratios. Rocks measured totaled 3314.

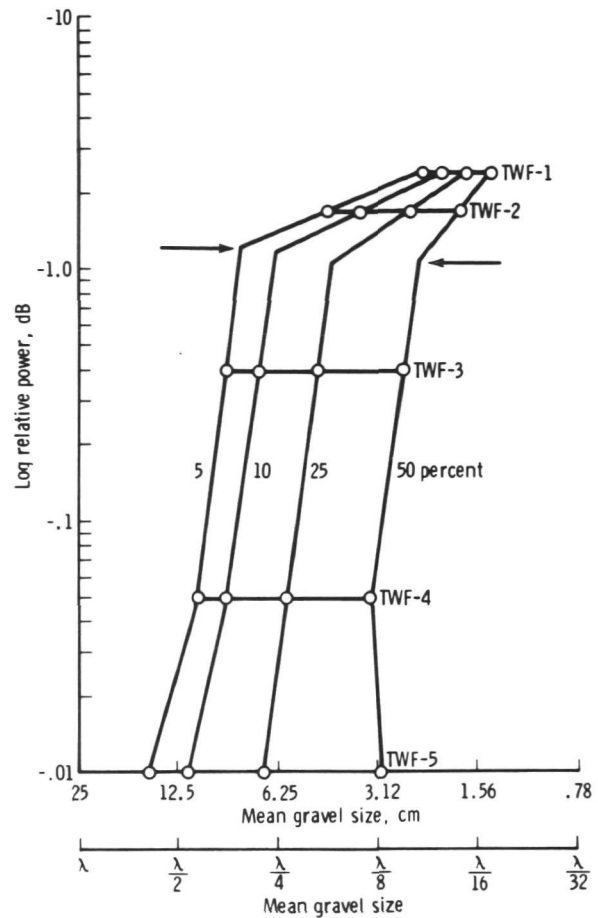


FIGURE 5-40.—Log relative power as a function of mean gravel size for TWF-1 to TWF-5 samples. Size distributions for 5, 10, 25, and 50 cumulative percent are shown.

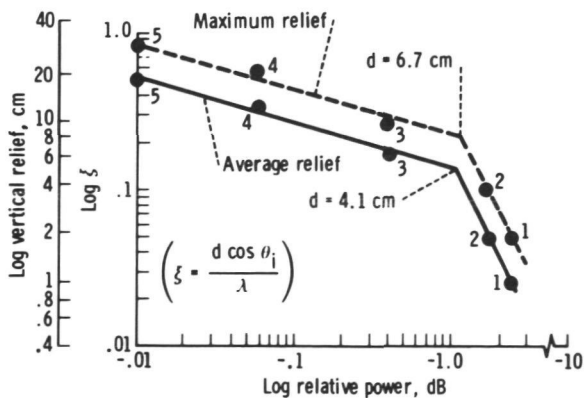


FIGURE 5-39.—Relative power variation as a function of average and maximum vertical reliefs for TWF-1 to TWF-5 sample sites (which are numbered 1 to 5).

are being conducted with that long-range goal in mind; however, the terrestrial benefits of such research studies are apparent.

The extremely good sensitivity of the radar system to variations in surface roughness appears to result from (1) the low frequency (1215 MHz); (2) the 45° to 90° antenna depression angle range, which emphasizes surface backscatter at the expense of conventional morphologic image portrayal; and (3) the high-resolution capability of the synthetic aperture system.

Surface moisture can substantially alter the complex dielectric constant and thus affect the backscatter power returned by sur-

face roughness alone. There are, however, an estimated 4×10^{10} m² of extremely arid land, 50×10^{10} m² of arid land, and 110×10^{10} m² of semiarid land within the limits of the contiguous 48 States (ref. 5-11). These relatively undeveloped regions could be the focal point of proposed airborne, Space Shuttle, and spacecraft radar-imaging applications such as the following:

1. Research on development of arid land recreational areas and other aspects of land use.
2. Detection of alluvial deposits for sand and gravel and for water potential.
3. Classification of active sedimentary processes (i.e., monitoring of aeolian activity and defining the extent of silt deposition after floodwaters recede).

Strategic Air Command, X-band (9500 MHz) SLAR images of Death Valley have been acquired recently. A full discussion and comparison of the X- and L-band images will be published in the near future; however, one enlargement of these high-resolution (15 m) X-band data is presented (fig. 5-41) for comparison with specific details on the L-band images.

The conspicuous dark band (unit V) around the base of the gravel fans on the L-band data (fig. 5-31) is present on the X-band image (fig. 5-41), but the area cannot be well delineated because of the less-distinctive tonal contrast between units V and III (the carbonate facies of the outer salt pan). Similarly, the contrast between units III and II on the X-band data is not as sharp as shown on the L-band images.

However, the desert pavement (unit VI) detail is somewhat better on the X-band image because this radar has a higher resolution and a more pronounced shadowing effect. The incident angle of the X-band data in the center of figure 5-41 is 72.3° , whereas the incident angle in the center of the L-band image (fig. 5-31) is 38.2° . The desert-pavement areas are very clearly defined on both radar frequencies as a result of the extremely smooth desert varnish surface (fig. 5-30). The pavement would probably be specular even on K-band images for this reason.

Within the salt pan, the X-band data appear to define geologic contacts between various chloride, sulfate, and carbonate facies differently than the L-band data. However, verification and discussion of the causal relationships must be delayed until further study of the X-band images is completed.

A SHUTTLE RADAR MICROWAVE SUBSYSTEM FOR EARTH RESOURCES APPLICATIONS

Introduction

The microwave subsystem considerations are discussed as a design example for a radar for Earth resources applications to be used in conjunction with the Shuttle Spacelab. This system with a multiplicity of frequencies and polarizations—L-band (25-cm wavelength), S-band (10-cm wavelength), and X-band (3.2-cm wavelength) at two orthogonal linear polarizations—has been tentatively selected. The Space Shuttle vehicle constrains the antenna to approximately 8 m in length and 3 m in width.

The frequencies and antenna size comprise the major constraints on the system described here and determine the sensor altitude, coverage, and major hardware parameters. The sensor performance is summarized as follows:

1. Frequencies:
 - a. L-band (25 cm)
 - b. S-band (10 cm)
 - c. X-band (3.2 cm)
2. Polarization:
 - a. Transmit: Vertical or horizontal
 - b. Receive: Vertical or horizontal
3. Imagery: Synthetic array; four looks in azimuth; 10-m range and azimuth resolution on the ground.
4. Coverage: Offset of 75 to 275 km either side of the satellite groundtrack.
5. Swath width:
 - a. At minimum offset: 40 km
 - b. At maximum offset: 100 km

The major microwave subsystem parameters are outlined as follows: